

# Modeling the Physical Properties of Environmentally-Friendly Optical Magnetic Switches: DFT and TD-DFT

Latévi Max LAWSON DAKU

*Université de Genève – Sciences II, Quai Ernest Ansermet 30, 1211 Genève, SUISSE*

Mark Earl CASIDA

*Laboratoire de Spectrométrie, Interactions et Chimie théorique (SITh), Département de Chimie Moléculaire (DCM, UMR CNRS/UGA 5250), Institut de Chimie Moléculaire de Grenoble (ICMG, FR2607), Université Grenoble Alpes (UGA) 301 rue de la Chimie, BP 53, F-38041 Grenoble Cedex 9, FRANCE*

---

## Abstract

The dominant majority of the hundreds of available spin-crossover compounds, including the technologically most promising ones, are based on the Earth-abundant metal iron, making these switches particularly appealing in terms of sustainable technology. Furthermore, it has recently been established that these materials may be synthesized using the techniques of Green Chemistry. Spin crossover in transition metal complexes can be induced by a change of temperature, by the application of an external pressure, or a magnetic field, and also by photoexcitation. Given the wide variety of functionalities to which these bistable photomagnetic systems could give access, they may be viewed as the prototypes of molecular-scale optomagnetic switches. Hence, in response to the growing demand for storing and treating increasingly-dense information, much effort has been devoted over several decades to the design of transition metal materials exhibiting spin crossover in technologically-accessible temperature ranges. The cornerstone for designing new efficient photoactive spin-crossover materials remains the ability to predict the magnetic behaviour and the photoresponse of any first-row transition complex, and the manner in which its properties are influenced by its environment. This is a challenge for the inorganic chemist and also, most notably, for the theoretical and the computational chemist. This chapter gives an overview of the issues tied to the application of DFT and TD-DFT to the characterisation of transition metal complexes in the framework of spin-crossover and related phenomena.

*Keywords:* Transition metal complexes, green chemistry, spin crossover, DFT, TD-DFT

---

---

*Email addresses:* [max.lawson@unige.ch](mailto:max.lawson@unige.ch) (Latévi Max LAWSON DAKU),

*Preprint submitted to Elsevier*

## 1. Introduction

In response to the growing demand for storing increasingly-dense information, an important effort is being made to develop new materials for information storage and processing at the molecular level. Transition-metal systems have a special role in this area because of their extremely diverse photophysical and photochemical properties and because of the possibility of coupling these photoproperties to magnetic properties. This is precisely the situation with spin-crossover (SCO) complexes as they may be reversibly switched between their low-spin ground state and their high-spin metastable excited state — two states with quite different optical and magnetic properties. The change of spin state may be induced by a change in temperature, by applying an external pressure or a magnetic field, or by photo-excitation. Given the vast range of functionalities which can in principle be accessed by these bistable photomagnetic systems, spin-crossover complexes may be considered to be the archetype of all optical magnetic switches. They have also been the object of many multidisciplinary studies, which have been reviewed in *Topics in Current Chemistry* [1]. Given that the dominant majority of the hundreds of available spin-crossover compounds, including the technologically most promising ones, are based on the Earth-abundant metal iron, these switches prove to be particularly appealing in terms of sustainable technology. Furthermore, mechanochemistry has recently been applied to the synthesis of SCO materials, thus demonstrating that these materials may be synthesized using the techniques of Green Chemistry [2].

The work of the authors on spin-crossover and “related” complexes has been carried out in the context of the study of photoswitching. A deeper understanding of this phenomenon requires the ability to answer the following key questions:

- (Q1) What is the nature of the states involved? (structures, energies, lifetimes, etc. ...)
- (Q2) How does the system interact with light? (excitation energies and electromagnetic transition moments)
- (Q3) How does the system evolve after photoexcitation?

Obtaining precise answers to these three questions is a major challenge to which we hope to contribute through the use of density-functional theory (DFT) and time-dependent DFT

---

mark.casida@univ-grenoble-alpes.fr (Mark Earl CASIDA)

(TD-DFT). This chapter gives an overview of problems related to the application of DFT and of TD-DFT to the study of spin-crossover complexes using examples taken principally from the work of the authors and the reader will be referred to the original papers for more detail.

This chapter is organized as follows: The next section presents a review of applicable methods with particular emphasis on DFT and on TD-DFT. In Sec. 3, stock is taken of the performance of different DFT functionals and it is shown that modern functionals can compete at a quantitative level with *ab initio* methods but at less computational cost. In Sec. 4, the application of TD-DFT to the study of the excited states of complexes is considered. In Sec. 5, the important subject of environmental effects on the behavior of spin-crossover complexes is tackled. Finally in Sec. 6 the authors conclude and try to imagine the future evolution of this field of study.

## 2. Methodology: Three Pauling Points

“Essentially, all models are wrong, but some are useful [3].” This quote from American statistician George E.P. Box, taken out of context, reminds us that models are, despite our best efforts, useful but necessarily imperfect. Very often, during the development of a model, the level of agreement between theory and experiment does not increase in a monotonic manner with increasing sophistication of the model but rather has a tendency to oscillate and local minima appear (Fig. 1.) In the folklore of theoretical chemistry, these local minima are frequently referred to as Pauling points because Linus Pauling (Nobel prizes: Chemistry, 1954; Peace, 1962) supposedly had the talent of stopping at these points [4].

Three Pauling points can be identified for spin-crossover complexes. The first is given by ligand field theory (LFT). This old but well-established semi-empirical theory is universally used to understand the behaviour of transition metal complexes [5]. It may be regarded as an essential and widely used language that experimentalists use to analyse their results using such concepts as ligand field strength, Racah parameters for describing electron repulsion, and the nephelauxetic effect, to mention just a few terms. Nevertheless LFT has several severe limitations. For example, LFT can provide only very limited quantitative indications regarding the molecular structure of a complex because the application of LFT typically involves first making some symmetry — and hence structural — assumptions about the complex. It is thus very difficult to obtain a detailed description of subtle variations in the spatial arrangement of ligands around the metal or to include environmental effects. Despite these difficulties, LFT is unavoidable, embodying as it does several decades of accumulated

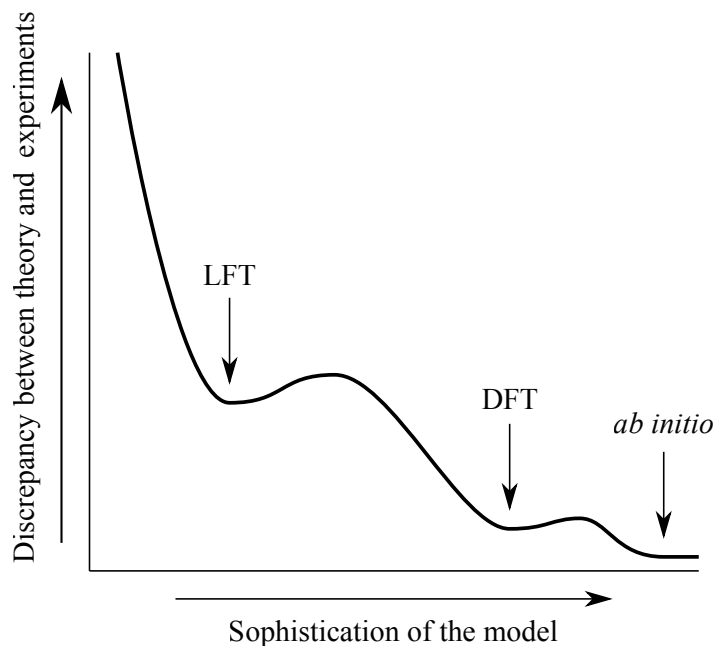


Figure 1: Evolution of the level of agreement between theory and experiment as a function of the sophistication of the theoretical model. The local minima where theory and experiment agree best are the Pauling points. In the spin-crossover case, we can distinguish three Pauling points (see Text).

experimental data.

The third Pauling point is given by *ab initio* calculations. The Latin term *ab initio* means “from the beginning” and means in the present context “from first principles.” It most often designates calculations based upon a single Slater determinant (Hartree-Fock) or on several Slater determinants carried out in a self-consistent manner, as for example the complete active space self-consistent field (CASSCF) method [6]. The self-consistent field (SCF) calculations must be supplemented with post-SCF calculations in order to recover important residual dynamic electron correlation effects. High-level coupled-cluster methods are dynamic correlation methods able to give results in the complete basis set limit accurate to within  $1 \text{ kcal mol}^{-1}$  ( $350 \text{ cm}^{-1}$ ), the so-called chemical accuracy [7, 8]. Their disadvantage is that the computational resources required (their “computational cost”) grows extremely very rapidly with molecular size. For this reason, they are mainly applied to small transition metal complexes to obtain important reference data for assessing the performance of simpler methods such as DFT or of other *ab initio* methods [9, 10]. Other *ab initio* methods used in studying spin-crossover complexes are CASPT2 (which is CASSCF plus second-order perturbation theory [11, 12]) and spectroscopy-oriented configuration interaction (SORCI) methods [13–15]. The computational cost of the CASSCF/CASPT2 method limited the reli-

ability of pioneering work on spin-crossover complexes [16]. Thanks to advances in CASSCF methodology, much more reliable CASPT2 calculations have been reported; see Refs [17–20], for instance. Nevertheless we continue to remain pessimistic regarding rigorous *ab initio* treatment of molecular systems larger than, say, about 100 atoms. Also, for small molecules, a chemical accuracy better than 5 kcal mol<sup>-1</sup> (1750 cm<sup>-1</sup>) is quite difficult to obtain once the molecule contains a transition metal atom. We call this level of precision the “best expected accuracy for transition metal systems” (BEA-TMS). In what follows, it may be useful to keep in mind that BEA-TMS = 1750 cm<sup>-1</sup>! Meeting this level of accuracy is so challenging that certain *ab initio* methods go so far as to include some semi-empiricism in order to approach it [20–22].

The second Pauling point is the method which probably comes closest at the present time to Aristotle’s Golden Mean. This is density-functional theory (DFT; John Pople and Walter Kohn, 1998 chemistry Nobel prize). DFT has had several important predecessors [23–26]. Its modern formalism is based upon the two Hohenberg-Kohn theorems [27], the first of which states that the Hamiltonian of the molecule is determined up to an arbitrary additive constant by the ground-state charge density  $\rho$ . The second Hohenberg-Kohn theorem establishes that the ground-state energy and charge density may be determined by minimizing a functional (that is, a function of a function) of the density.

Although there is an explicit exact constructive formula for this functional [28], it is also impractical and so approximations must be used in practice. This is why by far the most practical applications of DFT are carried out using the Kohn-Sham formalism [29] where the density is expressed in terms of a set of self-consistent Kohn-Sham molecular orbitals. In Kohn-Sham DFT, the key quantity is the exchange-correlation (xc) energy,  $E_{xc}[\rho]$ , which is a functional of the charge density  $\rho$  and is intended to describe missing exchange, correlation, and kinetic energy contributions which would otherwise be missing in an exact treatment. Again, as no practical exact form of the  $E_{xc}$  functional is known, it must be approximated in practice.

The starting point of nearly every approximation for  $E_{xc}$  is the homogeneous electron gas (HEG or “jellium”) for which very precise analytic forms are known for the xc-energy per particle. The local density approximation (LDA) consists of the assumption that the xc-energy of a system with an inhomogeneous density is locally the same as that in a HEG of the same charge density as at that point of the inhomogeneous system. This approximation works surprisingly well for optimizing molecular geometries and calculating vibrational frequencies. But the LDA tends to overestimate bond energies and to underestimate bond

lengths. One way to go beyond the LDA is to include a dependence on the gradient of the density in the form of the xc-energy functional through what are known as generalized gradient approximations (GGAs). These improve both bond energies and bond lengths. Unfortunately it is difficult to do better within the framework of the pure Kohn-Sham formalism where the only functional dependence permitted for the xc-energy functional is on the density. The present tendency is to extend the functional dependence of the xc-energy functional also to Kohn-Sham orbitals which are themselves implicit functionals of the charge density. Perdew has summarized the present hierarchy of functionals in a Jacob’s ladder [30, 31] shown in Table 1. Climbing *up* the ladder allows the designer of new functionals more flexibility in designing the xc-energy functional and hence more degrees of freedom to use to obtain better agreement between theory and experiment. But this better agreement is by no means guaranteed (though this is the observed tendency). All that is really guaranteed is that the calculations will become systematically more expensive. It is thus important to be able to also climb *down* Jacob’s ladder. For more information about DFT, the authors recommend the following books in order of increasing difficulty [32–34].

Table 1: Jacob’s ladder of density functionals [30, 35] (an updated version is given in Ref. [31]; adapted from Ref.[35])

Quantum Chemistry Heaven		
double-hybrid	—	$\rho(\mathbf{r}), x(\mathbf{r}), \tau(\mathbf{r}), \psi_i(\mathbf{r}), \psi_a(\mathbf{r})^h$
hybrid	—	$\rho(\mathbf{r}), x(\mathbf{r}), \tau(\mathbf{r}), \psi_i(\mathbf{r})^g$
mGGA <sup>c</sup>	—	$\rho(\mathbf{r}), x(\mathbf{r}), \tau(\mathbf{r})^e, \nabla^2\rho(\mathbf{r})^f$
GGA <sup>b</sup>	—	$\rho(\mathbf{r}), x(\mathbf{r})^d$
LDA <sup>a</sup>	—	$\rho(\mathbf{r})$
Hartree Model World		

<sup>a</sup> LDA, see text. <sup>b</sup> GGA, see text. <sup>c</sup> Meta GGA. <sup>d</sup> The reduced gradient  $x(\mathbf{r}) = |\vec{\nabla}\rho(\mathbf{r})|/\rho^{4/3}(\mathbf{r})$ . <sup>e</sup> The local kinetic energy density  $\tau(\mathbf{r}) = \sum_p n_p \psi_p(\mathbf{r}) \nabla^2 \psi_p(\mathbf{r})$ . <sup>f</sup> There are indications that the local kinetic energy density,  $\tau(\mathbf{r})$ , and the Laplacian of the charge density,  $\nabla^2\rho(\mathbf{r})$ , contain similar information [36]. <sup>g</sup>Occupied orbitals. <sup>h</sup>Unoccupied orbitals.

As originally formulated DFT is limited to the study of the ground-state time-independent properties. The best one might hope within the conventional formulation is that it will apply to the lowest state of each space and spin symmetry representation, although present-day xc-functionals do not have the symmetry dependence that would be rigorously required by such a generalization [37–39]. Time-dependent DFT (TD-DFT) is intended to treat time-dependent problems and also excited states. It is based upon theorems analogous to those

of Hohenberg and Kohn and has an associated time-dependent Kohn-Sham equation [40]. Once again the xc-functional is unknown and so must be approximated. One approximation which is made so often as to virtually define conventional TD-DFT is to assume that the self-consistent field in the TD Kohn-Sham equation acts instantaneously and without memory to any time-dependent change in the charge density. This so-called adiabatic approximation allows us to use functionals developed for ordinary ground-state static DFT as xc-functionals in TD-DFT. Excited states may be accessed by examining the response of the ground state to a time-dependent perturbation. Response theory then leads to the equation,

$$\begin{bmatrix} \mathbf{A}(\omega_I) & \mathbf{B}(\omega_I) \\ \mathbf{B}^*(\omega_I) & \mathbf{A}^*(\omega_I) \end{bmatrix} \begin{pmatrix} \vec{X}_I \\ \vec{Y}_I \end{pmatrix} = \omega_I \begin{bmatrix} \mathbf{1} & \mathbf{0} \\ \mathbf{0} & -\mathbf{1} \end{bmatrix} \begin{pmatrix} \vec{X}_I \\ \vec{Y}_I \end{pmatrix}, \quad (1)$$

whose solution gives molecular electronic absorption spectra [41]. Here the  $\omega_I$  (or more precisely  $\hbar\omega_I$ ) are the vertical excitation energies and the corresponding oscillator strengths,  $f_I$ , are calculated from the vectors  $\vec{X}_I$  and  $\vec{Y}_I$ . For more information regarding TD-DFT, the reader is referred to pertinent reviews [35, 41–45] and books [46, 47].

Finally, let us note that one of the challenges of modelling spin-crossover systems is to be able to treat larger and larger systems. The ideal method should be both simple and accurate, but with a computational difficulty which increases relatively slowly as the system grows. It is thus encouraging that DFT is particularly well adapted as a so-called  $\mathcal{O}(N)$  (order-N) method whose computational difficulty scales in direct proportion to the number of atoms [48] and there is every reason to believe that TD-DFT can be also made  $\mathcal{O}(N)$ .

### 3. Application of DFT to the Study of the Structure and Energetics of Transition-Metal Complexes in their High- and Low-Spin States

This section discusses the performance of DFT for describing the structural and energetic properties of low-spin (LS) and high-spin (HS) transition metal complexes. The discussion will be limited to hexacoordinate Fe(II) ( $d^6$ ) complexes. The ground state of such an octahedral ( $O_h$ ) complex has, according to ligand field theory, a LS singlet  $^1A_{1g}(t_{2g}^6)$  state characterized by maximum spin pairing of the  $d$  electrons in the presence of strong-field ligands, and a HS quintuplet  $^5T_{2g}(t_{2g}^4e_g^2)$  characterized by minimal  $d$ -electron pairing in the presence of weak field ligands. Orbital degeneracy is lifted by structural distortions due to the Jahn-Teller effect, but these are typically weak for  $O_h$  HS  $d^6$  complexes. The performance of DFT for the determination of the geometries of LS and HS complexes will be

examined first, then its performance for the HS-LS energy difference. It will be seen that the quality of xc-functionals is particularly important when it comes to determining the relative energetics of the spin states of these complexes.

### 3.1. Performance of DFT for calculating the geometries of LS and HS complexes

Table 2: Comparison of theoretical and experimental average Fe-O distances ( $\text{\AA}$ ) for the complex  $[\text{Fe}(\text{H}_2\text{O})_6]^{2+}$ . The computational method is indicated in the form “computational method/basis set used” (where the name of the basis set is the same as that used in the cited article). Exchange-, correlation-, and exchange-correlation-type functionals are designated, respectively by x, c, and xc. Functionals are typically named by the abbreviation for the exchange part followed by the name for the correlation part (e.g., PB86 is composed of the x-GGA B and the c-GGA P86). Further information about abbreviations used in describing functionals is given in Table 1 and the associated discussion in Sec. 2

Method	$r_{\text{LS}}$	$r_{\text{HS}}$	$\Delta r_{\text{HL}}$
LDA/A <sup>a</sup> :1965 <sup>A</sup> (x-LDA) [29]	1.912	2.070	0.158
BP86/E <sup>a</sup> : 1988 (x-GGA) [49] + 1986 (c-GGA) [50]	1.996	2.145	0.149
BLYP/E <sup>a</sup> :1988 (x-GGA) [49] + 1988 (c-GGA) [51]	2.025	2.166	0.141
PW91/E <sup>a</sup> : 1991 (xc-GGA) [52] <sup>B</sup>	1.992	2.137	0.145
PBE/C <sup>a</sup> : 1996 (xc-GGA) [53]	2.011	2.154	0.143
RPBE/C <sup>a</sup> : 1999 (x-GGA) [54] + 1996 (c-GGA) [53]	2.048	2.187	0.139
B3LYP/E <sup>a</sup> : 1994 (xc-hybrid) <sup>C</sup>	2.018	2.154	0.136
Hartree-Fock <sup>b</sup>	2.080	2.193	0.113
CASSCF(10,12)/II <sup>b</sup>	1.989	2.113	0.124
CASSCF(12,10) <sup>a</sup>	2.077	2.186	0.119
Exp. <sup>a</sup>	—	2.068-2.156	—
LFT <sup>c</sup>	—	—	0.126

<sup>A</sup> VWN parameterization of the c-LDA functional [55]. <sup>B</sup> The PW91 functional was first presented in a DFT conference and then became rapidly incorporated into many DFT codes through sharing of an implementation of the functional as a FORTRAN subroutine. Interestingly no official publication describing the functional appeared for quite a while. <sup>C</sup> The B3LYP functional is the same as the hybrid functional proposed by Becke [56], except that the c-GGA P91 functional has been arbitrarily replaced by the c-GGA LYP [51] functional without any reoptimization of parameters. <sup>a</sup> Results taken from Ref. [57]. <sup>b</sup> Ref. [17]. <sup>c</sup> This LFT estimate is described in Ref. [58].

Geometries obtained with DFT for LS and HS transition metal complexes are generally rather good. In order to discuss this concretely, let us take the case of the complex  $[\text{Fe}(\text{H}_2\text{O})_6]^{2+}$ . This complex is referred to as HS because the HS electronic ground state, which is entropically favored, remains the only populated state at all temperatures. Of course, the metastable LS state can be examined theoretically. Geometry optimizations of the HS state with different functionals lead to a nondegenerate quintuplet with a geometry which is only slightly distorted due to the Jahn-Teller effect. For the LS state, these optimizations lead to a nondegenerate state of  $O_h$ -symmetry. In order to describe these structures,

the focus will be put on the mean Fe-O bond length which is given in Table 2 for the HS ( $r_{\text{HS}}$ ) and LS ( $r_{\text{LS}}$ ) states. As  $[\text{Fe}(\text{H}_2\text{O})_6]^{2+}$  is a HS species, only the structure of the HS state has been characterized experimentally, both in solution and in crystals. The experimental values given in Table 2 vary by almost 0.09 Å: this great variation emphasizes the importance of environmental effects on the properties (structural in this case) of the complexes. There is a large lengthening of the metal-ligand bond distance after the LS  $\rightarrow$  HS change of state as the result of the promotion of two electrons from the nonbonding  $t_{2g}$  orbitals to the antibonding  $e_g$  orbitals.

The absence of experimental data for LS  $[\text{Fe}(\text{H}_2\text{O})_6]^{2+}$  and the fact that the calculations are for gas phase molecules while experimental measurements are for molecules in condensed phases means that it is difficult to know which of the predicted  $r_{\text{LS}}$ ,  $r_{\text{HS}}$ , and  $r_{\text{HL}}$  values should be taken as most reliable. Nevertheless all values are in good agreement with what is known experimentally, especially if we take into account the probable compression of the molecule in the condensed phase. This level of agreement confirms the earlier claim that one of the strengths of DFT is the high quality of optimized geometries, which allows one to go well beyond simple LFT. The performance of different types of functionals can also be compared. The LDA tends to overestimate the bond energy. This is seen here by the fact that, compared to other functionals, the LDA is giving Fe-O bond distances which are too short. Consistent with their historical purpose, the GGAs correct the overbinding of the LDA and give longer bonds. Hybrid functionals incorporate a contribution of HF exchange into the GGA form. As represented here by the hybrid functional B3LYP, hybrid functionals yield geometries which are similar to those obtained with GGAs.

Although different functionals give similar HS and LS optimized geometries, there are important variations of up to 40% in the difference  $\Delta r_{\text{HL}}$ . Generally speaking it is difficult to say which functional is best for calculating geometries, either because the theoretical calculations are of gas-phase geometries which cannot be directly compared with condensed-phase measurements or because the molecules are too large to optimize using high-quality *ab initio* methods. In the specific case of  $[\text{Fe}(\text{H}_2\text{O})_6]^{2+}$ , if one believes the LFT estimation for  $\Delta r_{\text{HL}}$  (which is based upon decades of empirical experience) and the CASSCF calculations, then the HF results (which lack electron correlation) and LDA calculations can be ruled out in favor of DFT calculations with GGAs or hybrid functionals. This conclusion is also expected to hold for most transition metal complexes.

### 3.2. Performance of DFT for spin-crossover energies

When considering the HS-LS energy difference, one needs to distinguish between the HS-LS zero-point energy difference,  $\Delta E_{\text{HL}}^{\circ} = E_{\text{HS}}^{\circ} - E_{\text{LS}}^{\circ}$ , its electronic contribution,  $\Delta E_{\text{HL}} = E_{\text{HS}} - E_{\text{LS}}$ , and its vibrational contribution,  $\Delta E_{\text{HL}}^{\text{v}} = E_{\text{HS}}^{\text{v}} - E_{\text{LS}}^{\text{v}}$  ( $\Delta E_{\text{HL}}^{\circ} = \Delta E_{\text{HL}} + \Delta E_{\text{HL}}^{\text{v}}$ ).  $\Delta E_{\text{HL}}$  can be obtained by optimizing HS and LS geometries, while  $\Delta E_{\text{HL}}^{\circ}$  requires additional vibrational frequency calculations for the HS and LS complexes. Density-functional calculations with GGA or hybrid functionals typically give very good frequencies for complexes and hence good estimates of  $\Delta E_{\text{HL}}^{\text{v}}$ . The situation is more complicated when it comes to determining  $\Delta E_{\text{HL}}$  which, in spin-crossover complexes, takes values on the order of  $100 \cong 1000 \text{ cm}^{-1}$ . For such calculations, the best *ab initio* methods have a BEA-TMS of around  $1750 \text{ cm}^{-1}$  (Sec. 2). This is thus quite a challenge for DFT.

The current situation may be summed up in the following way. Hartree-Fock tends to strongly underestimate  $\Delta E_{\text{HL}}$ . The LDA functional tends to strongly overestimate  $\Delta E_{\text{HL}}$ . The GGAs tend to correct the problems with the LDA. But DFT calculations prior to the beginning of this century tended to overestimate the stability of the LS state with respect to the HS state. The same studies showed that the B3LYP hybrid functional, which was the most sophisticated widely-used functional at that time, overestimated the stability of the HS state with respect to the LS state. Thus  $\Delta E_{\text{HL}}$  is underestimated as with the HF method. The beginning of the 2000s saw a significant increase in the performance of density functionals. One example was the B3LYP\* functional obtained by empirically decreasing the amount of HF exchange in the B3LYP functional from 20% to 15% so as to reproduce the ground states of a series of complexes [64]. It is important to be able to descend Jacob’s ladder (Sec. 2), and the advent of new and more sophisticated GGAs seemed to offer interesting new possibilities. In fact, when it came to testing the ability of these functionals for calculating  $\Delta E_{\text{HL}}$ , the biggest problem was to collect and verify reliable comparison data. This is far from trivial because electronic structure calculations are usually made for the isolated complex while experimental data is often for complexes in condensed media and hence have a different enthalpy and free energy dependence than in the gas phase. For example, Table 3 gives results obtained for the values of  $\Delta E_{\text{HL}}$  for the complexes  $[\text{Fe}(\text{H}_2\text{O})_6]^{2+}$ ,  $[\text{Fe}(\text{NH}_3)_6]^{2+}$ , and  $[\text{Fe}(\text{bpy})_3]^{2+}$  (bpy = 2,2’-bipyridine). Quality benchmarks have been obtained for the small HS complexes  $[\text{Fe}(\text{H}_2\text{O})_6]^{2+}$  [57] and  $[\text{Fe}(\text{NH}_3)_6]^{2+}$  by high-level *ab initio* CASPT2 and SORCI calculations [57, 58]. As to the LS complex  $[\text{Fe}(\text{bpy})_3]^{2+}$ , a reliable estimation of  $\Delta E_{\text{HL}}$  has been obtained by an experimental study of the HS  $\rightarrow$  LS relaxation rate of the complex in different solid matrices [59, 67].

Table 3: Comparison of the energy difference  $\Delta E_{\text{HL}} = E_{\text{HS}} - E_{\text{LS}}$  for different functionals ( $\text{cm}^{-1}$ ) for well-characterized iron(II) complexes. The spin of the ground state is given in parentheses. For the  $D_3$  complex  $[\text{Fe}(\text{bpy})_3]^{2+}$  (bpy = 2,2'-bipyridine), note that the  ${}^5E$  and  ${}^5A_1$  are quasidegenerate [59] and correspond to the  ${}^5T_{2g}$  LFT state. We take the HS LFT state to be the lower energy  ${}^5A_1$  state in this case. The functionals are listed in chronological order

Method	Molecule		
functional: year (type) [reference]	$[\text{Fe}(\text{H}_2\text{O})_6]^{2+}$ (HS)	$[\text{Fe}(\text{NH}_3)_6]^{2+}$ (HS)	$[\text{Fe}(\text{bpy})_3]^{2+}$ (LS)
LDA: 1965 <sup>A</sup> (Local-x) [29]	-3 896 <sup>a</sup>	8 187 <sup>b</sup>	
BP86: 1988 (GGA-x) [49]			
+ 1986 (GGA-c) [50]	-8798 <sup>a</sup>	790 <sup>b</sup>	11135 <sup>d</sup>
PW91: 1991 (GGA-xc) [52] <sup>B</sup>	-9232 <sup>a</sup>	617 <sup>b</sup>	11887 <sup>d</sup>
B3LYP: 1994 (Hybrid-xc)[,] <sup>C</sup>	-11465 <sup>a</sup>	-4 978 <sup>b</sup>	1211 <sup>d</sup>
PBE: 1996 (GGA-xc) [53]	-10081 <sup>a</sup>	-147 <sup>b</sup>	11337 <sup>d</sup>
HCTH93: 1998 (GGA-xc) [60]	-18779 <sup>b</sup>	-9430 <sup>b</sup>	
HCTH147: 1998 (GGA-xc) [60]	-18211 <sup>b</sup>	-8576 <sup>b</sup>	
HCTH407: 1998 (GGA-xc) [60]	-19631 <sup>b</sup>	-10682 <sup>b</sup>	
VSXC: 1998 (meta-GGA-xc) [61]	-13975 <sup>e,f</sup>	-5928 <sup>e,f</sup>	-1822 <sup>e,f</sup>
RPBE: 1999 (GGA-xc) [54]	-11844 <sup>a</sup>	-2744 <sup>b</sup>	6640 <sup>d</sup>
PBE0 <sup>D</sup> : 1999 (Hybrid-xc) [62]	-14504 <sup>b</sup>	-7195 <sup>b</sup>	-466 <sup>d</sup>
OLYP <sup>E</sup> : 2001 (GGA-x) [63]			
+ 1988 (GGA-c) [51]	-16284 <sup>e,f</sup>	-6693 <sup>e,f</sup>	2684 <sup>e,f</sup>
OPBE <sup>E</sup> : 2001 (GGA-x) [63]			
+ 1988 (GGA-c) [53]	-17200 <sup>g</sup>	-6650 <sup>g</sup>	5210 <sup>g</sup>
B3LYP*: 2002 (Hybrid-xc) [64]	-10456 <sup>e,f</sup>	-3226 <sup>e,f</sup>	3332 <sup>e,f</sup>
Best Estimates			
Exp.			3500 — 6000 <sup>d</sup>
<i>Ab initio</i> <sup>c</sup>	-13360 — -12347 <sup>a</sup>	-11230 — -9125 <sup>b</sup>	
Average	-12853	-10177	4750

<sup>A-C</sup> See Table 2. <sup>D</sup> Also known as PBE1PBE. <sup>E</sup> The OPTX GGA-x [63] is often designated by the letter O, as in the xc-functionals OLYP and OPBE. <sup>a</sup> Ref. [57]. <sup>b</sup> Ref. [58]. <sup>c</sup> Results of CASPT2 and SORCI calculations with empirical atomic energy correction [57, 58]. <sup>d</sup> Ref. [59]. <sup>e</sup> Ref. [65]. <sup>f</sup> At the geometry optimized using the same functional for these complexes. Note that the choice of functional has relatively little effect on the geometry optimizations. <sup>g</sup> Ref. [66].

The uncertainty of the *ab initio* results is  $1013\text{ cm}^{-1}$  for the  $[\text{Fe}(\text{H}_2\text{O})_6]^{2+}$  complex and  $2105\text{ cm}^{-1}$  for the  $[\text{Fe}(\text{NH}_3)_6]^{2+}$  complex, which is consistent with the BEA-TMS of  $1750\text{ cm}^{-1}$ . The uncertainty of the experimental value found for the  $[\text{Fe}(\text{bpy})_3]^{2+}$  complex is larger ( $2\ 500\text{ cm}^{-1}$ ), reflecting the influence of the environment on  $\Delta E_{\text{HL}}$ . The LDA and the GGAs before 1998 (BP86, PW91, RPBE) overestimate the difference  $\Delta E_{\text{HL}}$ . Also, for  $[\text{Fe}(\text{bpy})_3]^{2+}$ ,  $\Delta E_{\text{HL}}$  is underestimated for the classic hybrids B3LYP and PBE0. This is different than the case of the  $[\text{Fe}(\text{H}_2\text{O})_6]^{2+}$  complex for which  $\Delta E_{\text{HL}}$  is underestimated by PBE0 but which is nevertheless given reasonably well by the B3LYP functional. Finally, the two hybrid functionals both overestimate the best estimate of  $\Delta E_{\text{HL}}$  for  $[\text{Fe}(\text{NH}_3)_6]^{2+}$ . The reparameterized functional B3LYP\* gives a distinct improvement over the original B3LYP functional for  $\Delta E_{\text{HL}}$  for  $[\text{Fe}(\text{bpy})_3]^{2+}$ . On the other hand, B3LYP\* is even worse than B3LYP in so far as B3LYP\* results in a greater overestimation of  $\Delta E_{\text{HL}}$  than does B3LYP for the  $[\text{Fe}(\text{H}_2\text{O})_6]^{2+}$  and  $[\text{Fe}(\text{NH}_3)_6]^{2+}$  complexes which are, after all, chemically very different than the complexes originally used to parameterize the B3LYP\* functional. The post-1996 functionals such as RPBE, the ‘‘HCTH’’ functionals, and the OLYP and OPBE functionals give better results than previous GGAs. The OLYP and OPBE functionals differ only by the correlation functionals whose choice is less important for the relative spin energies than is that of the exchange functional. At the present time, these two GGAs are two of the best performing functionals for iron(II) complex spin-state energetics. Thus, the OLYP gives better results than B3LYP\* for the calculation of free energy differences  $\Delta G_{\text{HL}}$  in the series originally used to parameterize the B3LYP\* functional [65]. In fact, it would appear that the contribution of HF exchange in the B3LYP\* functional should be further decreased below its current value of 15% in order to improve the performance of this hybrid [65, 68]. The dependence of  $\Delta E_{\text{HL}}$  with respect to the contribution of HF exchange has also been studied in the case of  $[\text{Fe}(\text{bpy})_3]^{2+}$ . The results in this latter case suggest that the proportion of HF exchange should be reduced to around 10% not just in the B3LYP functional but also in the PBE0 functional [59]. Also note that a study has shown the OPBE functional to perform well for spin-state energetics in iron(II) and iron(III) complexes [66].

It would seem that in going from the B3LYP\* to the OLYP and OPBE GGAs that Jacob’s ladder has been successfully descended without any noticeable loss of precision. One may thus envisage with confidence studying much larger transition metal compounds than those studied here. Further improvement of spin-state energetics is likely to continue as long as work continues to design better and better density functionals.

A major problem linked to the use of DFT for spin-state energetics is that it is difficult

and risky to anticipate the performance of a functional for spin-crossover complexes on the basis of its good – even excellent – performance for other complexes. It would thus be interesting to be able to estimate  $\Delta E_{\text{HL}}$  by somehow avoiding the functional dependence. Thus, supposing that the different xc-functionals give very similar potential energy surfaces which are nevertheless shifted in energy with respect to each other, it has been shown [69] that the difference  $\Delta(\Delta E_{\text{HL}})$  of the  $\Delta E_{\text{HL}}$  energy differences for the two complexes  $C_1$  and  $C_2$ ,  $\Delta(\Delta E_{\text{HL}}) = \Delta E_{\text{HL}}(C_1) - \Delta E_{\text{HL}}(C_2)$ , should be roughly independent of the choice of functional. This hypothesis has been verified by calculations on two iron(II) spin-transition complexes using 53 functionals including GGAs, hybrid, and meta-GGAs [69]. The GGAs used gave results in very good agreement with the hypothesis while the hybrids were in less good agreement with the hypothesis and the meta-GGAs failed completely. Nevertheless it seems possible, knowing  $\Delta E_{\text{HL}}$  for a reference complex, to use DFT calculations to estimate its value for other complexes with a precision similar to, or possibly even better than, the BEA-TMS [69, 70].

#### 4. Excited States from TD-DFT

Among the methods for describing molecular excited states, TD-DFT is probably the one which is currently the most used for studying large and middle-sized molecules. For reasons of brevity, only a few observations will be made on the place of TD-DFT in the study of transition metal complexes, and particularly spin-crossover complexes.

A very important field of application of TD-DFT is modeling the photophysical properties of ruthenium(II) complexes, which are  $d^6$  closed-shell complexes which are of interest for several reasons, including the fact that they are used as photosensitizers in Grätzel’s dye-sensitized photocells [71]. In fact, the number of papers reporting TD-DFT calculations for this particular application has really taken off, in part, because of the ready availability of the method in the vast majority of quantum chemistry and quantum physics programs as well as because of the good agreement obtained between theory and experiment with this approach.

In fact, as far as the application of TD-DFT to closed shell ruthenium(II) complexes around their equilibrium geometries, the situation is relatively simple in the sense that one essentially needs only concern oneself with the choice of the functional to use.<sup>1</sup> Moreover

---

<sup>1</sup>An atomic orbital basis set must also be chosen so as to give an adequate description of the Kohn-Sham molecular orbitals, but the basis set problem is shared by TD-DFT and excited-state *ab initio* methods. In general larger basis sets may be used in TD-DFT calculations than in sophisticated excited-state *ab initio* methods.

most GGA and hybrid functionals give a good description of the valence excited states of these molecules. However, the domain of validity of TD-DFT for practical calculations is limited by the approximate nature of these functionals and the use of the TD-DFT adiabatic approximation (Sec. 2), TD-DFT is not without its limitations. For example, the characterization of high-energy (Rydberg) excited states requires the use of functionals whose xc-potentials have the correct asymptotic behavior. Also there are problems describing charge-transfer excitations and those with significant multiple-excitation character. The reader seeking more information about the strengths and limitations of TD-DFT and how the limitations may be attenuated or eliminated altogether are referred to Refs. [35, 41–47, 72–81] for more detailed information.

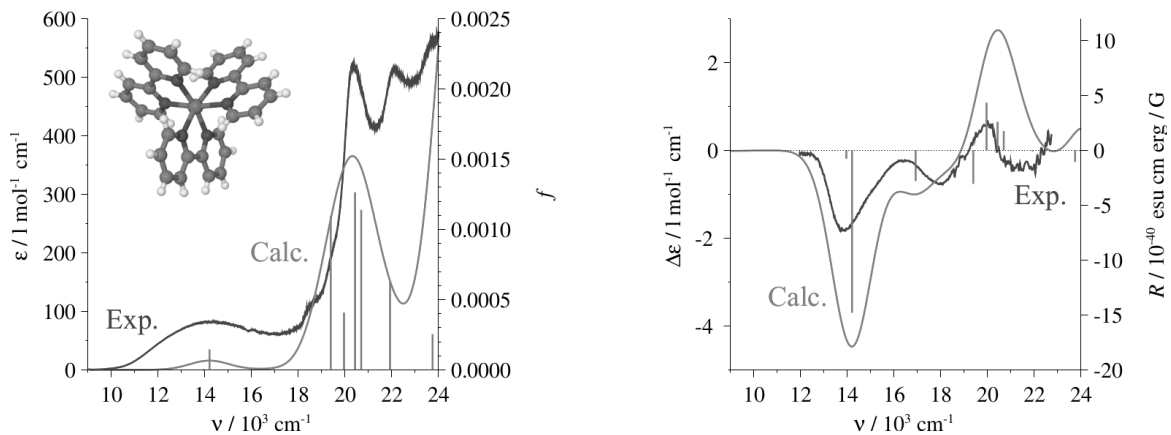


Figure 2: Absorption (left) and circular dichroism (right) spectra calculated for the  $\Lambda$  enantiomer of the  $[\text{Co}(\text{bpy})_3]^{2+}$  complex in the LS state (TDB3LYP/TZVP calculation.) Also shown are the measured absorption and dichroism spectra for a single crystal of  $[\text{Co}(\text{bpy})_3][\text{LiRh}(\text{ox})_3]$  at respectively 11 K and 15 K. Figure adapted from Ref. [82].

TD-DFT may also be used to study the optical properties of open-shell species such as the  $d^7$  complex  $[\text{Co}(\text{bpy})_3]^{2+}$ . The absorption and circular dichroism spectra of this chiral complex were calculated at the TD-B3LYP/TZVP level [82]. Figure 2 shows that the spectra obtained for the  $\Lambda$  enantiomer of the LS complex, while taking into account the Jahn-Teller instability of this state (see Ref. [82]). The calculated oscillator strengths and rotatory power (see below) are each represented by stick spectra. To simulate the absorption spectrum  $\epsilon = \epsilon(\tilde{\nu})$  ( $\epsilon$  in  $\text{M}^{-1} \text{cm}^{-1}$ ,  $\tilde{\nu}$  in  $\text{cm}^{-1}$ ), the molar extinction coefficient  $\epsilon_I(\tilde{\nu})$  associated with the  $I$ th transition centered at  $\tilde{\nu}_I$  has been calculated by convoluting the oscillator strength  $f_I$  with a gaussian with a full-width at half-height of  $2\,000 \text{ cm}^{-1}$

whose normalization guarantees the equality,

$$f_I = (4.32 \times 10^{-9} \text{ M cm}^2) \int \epsilon_I(\tilde{\nu}) d\tilde{\nu}. \quad (2)$$

The rotatory power  $R_I$  of this transition is related to the difference  $\Delta\epsilon_I$  between the absorption coefficients for left-circularly polarized light ( $\epsilon_g$ ) and right-circularly polarized light ( $\epsilon_d$ ) ( $\Delta\epsilon = \epsilon_g - \epsilon_r$ ), by the relation,

$$R_I = (22.97 \times 10^{-40} \text{ cgs M cm}) \int_0^\infty \frac{\Delta\epsilon(\tilde{\nu})}{\tilde{\nu}} d\tilde{\nu}. \quad (3)$$

In order to model circular dichroism spectra,  $\Delta\epsilon_I(\tilde{\nu})$  has been calculated by convoluting the rotatory power  $R_I$  using a Gaussian whose full width at half height is  $2\,000 \text{ cm}^{-1}$  and whose normalization guarantees the above equality. Figure 2 compares the calculated spectra with those measured for a monocrystal of the spin-crossover compound  $[\text{Co}(\text{bpy})_3][\text{LiRh}(\text{ox})_3]$  which is LS at the cryogenic temperatures used in the measurement. The agreement between theory and experiment is quite good. This allows to identify the configuration of the  $[\text{Co}(\text{bpy})_3]^{2+}$  complex as  $\Lambda$  [82].

Although TD-DFT provides a semiquantitative way to predict the envelope of the spectrum, it does not necessarily allow to do this by giving a good description of the underlying states. This depends upon the quality of the functional used and, for open-shell systems, on the degree of spin-contamination. The TD-DFT study of open-shell systems may suffer from complications due to spin contamination in the ground or in the excited states. Spin contamination occurs when the approximate wave function  $\Psi$  used to describe the  $S$  spin state is not an eigenfunction of the spin operator  $\hat{\mathbf{S}}^2$  with corresponding eigenvalue  $S(S+1)$ . The diagnosis of the degree of spin contamination is obtained by calculating  $\langle \hat{\mathbf{S}}^2 \rangle = \langle \Psi | \mathbf{S}^2 | \Psi \rangle$  and comparing it with the expected value of  $S(S+1)$ . The problem of spin contamination is typically less important in DFT than in Hartree-Fock calculations. In TD-DFT calculations, its complete (or partial) absence is a necessary, but not sufficient, condition for the correct description of the excited state.

Thanks to recent work [35, 83–85], there are now tools which allow to automatically assign the spin of excited states in TD-DFT, and thus to identify and eventually correct spin-contamination. Figure 3 illustrates this approach in the case of the  $[\text{Fe}(\text{H}_2\text{O})_6]^{2+}$  complex [86–89]. Potential energy curves are shown for the ground ( $Q_0$ ) and excited ( $Q_{I \geq 1}$ ) quintuplet states of the  $[\text{Fe}(\text{H}_2\text{O})_6]^{2+}$  complex along the Fe-O distance associated with the totally symmetric breathing mode. The curves for the expectation values  $\langle \hat{\mathbf{S}}^2 \rangle$  calculated at the

same geometries are shown. The four lowest energy curves correspond to the ground and  $d \rightarrow d$  type excited states. These states are spin-contamination free ( $\langle \hat{S}^2 \rangle = 6$ ). The higher energy curves correspond to metal  $\rightarrow$  ligand charge transfer excitations. Depending upon the geometry of the complex these latter states show spin-contamination ( $\langle \hat{S}^2 \rangle = 7$ ) and must either be discarded or corrected to make them physical [84].

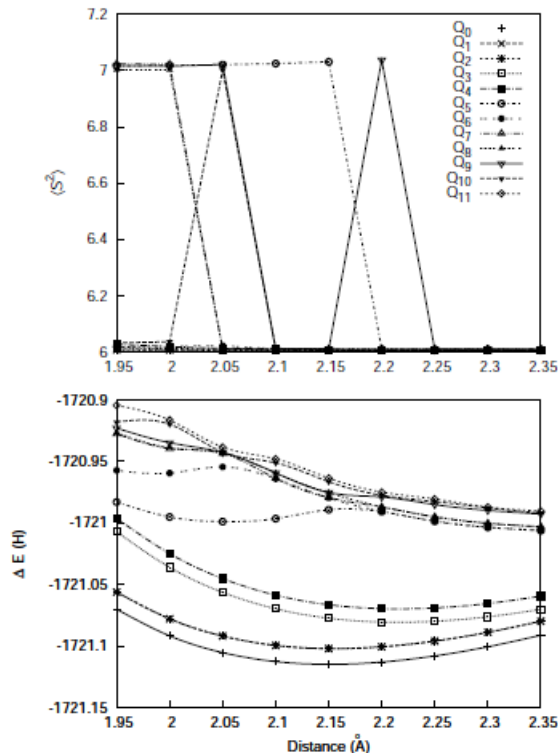


Figure 3: Potential energy curves for ground ( $Q_0$ ) and excited ( $Q_{T \geq 1}$ ) quintuplet states of the  $[\text{Fe}(\text{H}_2\text{O})_6]^{2+}$  complex along the Fe-O breathing coordinate  $[R(\text{Fe-O})]$  and the corresponding calculated expectation values  $\langle \hat{S}^2 \rangle$  calculated along the same potential energy curve. The DFT calculations have been calculated using the PBE functional for the ground state and using TD-DFT in the TDA and the adiabatic LDA for the excited states.

Spin-contamination is at least partially a consequence of the simplicity of TD-DFT in its current developmental state. But even this simplicity is very beneficial as it allows photodynamics modeling using Tully-type mixed TD-DFT/classical trajectory surface hopping [90–95]. The application to the photochemistry of oxirane of this technique for modeling nonadiabatic dynamics has been very instructive [90, 93]. It is currently believed that most photoreactions pass either through or near conical intersections and that nuclear dynamics is often needed in order to understand photoreaction products. It is hence essential for TD-DFT to be able to give a good description of systems near conical intersections. Con-

ventional TD-DFT uses the adiabatic approximation (i.e., the frequency dependence of the  $\mathbf{A}$  and  $\mathbf{B}$  matrices in Eq. (1) is neglected). A seminal TD-DFT study of oxirane has shown the importance of the Tamm-Dancoff approximation (TDA) [ $\mathbf{B}=0$  in Eq. (1)] to reduce the harmful effects of spin-instabilities in TD-DFT calculations of the potential energy surfaces [90]. Later it was seen that applying mixed TDA TD-DFT/classical trajectory surface hopping gave results in good agreement with known experimental results and provided a more complete understanding of the classic Gomer-Noyes mechanism of the reaction [93]. This was surprising from the point of view that conventional TD-DFT cannot provide true conical intersections between the ground and excited states [96]. Instead the potential energy surfaces obtained by TDA TD-DFT and CASSCF have almost the same appearance near the conical intersection determined by the CASSCF calculations except that the TDA TD-DFT has two slightly interpenetrating cones instead of a true conical intersection. This detail may be important for determining the surface hopping rate. But the results of Ref. [93] show that the TDA TD-DFT description is adequate for predicting the mechanism of the photoreaction.

## 5. Inclusion of Environmental Effects

Up to this point the focus has been put on the properties of isolated complexes. The influence of the environment of the complex is by no means anodine. Consider the case of hexacoordinated iron(II) complexes. Under a LS  $\rightarrow$  HS transition, their molecular volume increases considerably due to lengthening of the metal-ligand bonds (Table 2). This large volume change is the origin of the pressure sensitivity of spin-crossover and of the sensitivity of spin-crossover to modifications of the second coordination sphere of the complexes [67]. Thus the application of an external pressure destabilizes the HS state with respect to the LS state which has a smaller molecular volume, and hence also increases the zero-point energy difference  $\Delta E_{\text{HL}}^{\circ}$ . By analogy, the environmental influence on  $\Delta E_{\text{HL}}^{\circ}$  can also be rationalized in terms of “internal” or “chemical” pressure which destabilizes the HS state with respect to the LS state.

The value of  $\Delta E_{\text{HL}}^{\circ}$  determines not only the spin-crossover transition but also the kinetics of the HS  $\rightarrow$  LS intersystem crossing which follows the photoinduced population of the HS state. The HS  $\rightarrow$  LS relaxation is observed after photoexcitation for any LS iron(II) complex, such as typical spin-crossover systems or  $[\text{Fe}(\text{bpy})_3]^{2+}$ . At cryogenic temperatures, relaxation takes place through tunnelling. In so far as, for a chemically similar family of complexes, the structural change induced by a spin change may be mainly described as a

uniform change in metal-ligand distances, the relaxation rate constant in the tunnelling regime  $k_{\text{HL}}(T \rightarrow 0 \text{ K})$  may be written as a simple function of  $\Delta E_{\text{HL}}^\circ$  and of the change  $\Delta r_{\text{HL}}$  in the average metal-ligand bond length,  $k_{\text{HL}}(T \rightarrow 0 \text{ K}) = f(\Delta r_{\text{HL}}, \Delta E_{\text{HL}}^\circ)$  [97]. In the case of spin-crossover systems, the parameters  $\Delta r_{\text{HL}}$  and  $\Delta E_{\text{HL}}^\circ$  may be determined experimentally: Thus bond-length difference  $\Delta r_{\text{HL}}$  may be found by comparing crystal structures for LS and HS complexes. The energy difference  $\Delta E_{\text{HL}}^\circ$  is proportional to the spin-crossover temperature  $T_{1/2}$ .

Thus, for  $[\text{Fe}(\text{II})\text{N}_6]$  spin-crossover transition complexes, it is known that  $\Delta r_{\text{HL}}$  is about 0.2 Å and  $k_{\text{HL}}(T \rightarrow 0 \text{ K}) \approx g(\Delta E_{\text{HL}})$  [97]. Consequently, it is possible to estimate  $\Delta E_{\text{HL}}$  from  $k_{\text{HL}}(T \rightarrow 0 \text{ K})$  for any LS  $[\text{Fe}(\text{II})\text{N}_6]$ -type spin-crossover complex. This approach has been applied to the LS complex  $[\text{Fe}(\text{bpy})_3]^{2+}$  and it was found that  $2\,500 \text{ cm}^{-1} \leq \Delta E_{\text{HL}} \leq 5\,000 \text{ cm}^{-1}$ . To obtain this, as the crystallographic structure of the HS state of this LS complex is not known, it was necessary to make the ansatz that  $\Delta r_{\text{HL}} \approx 0.2 \text{ Å}$ . However this ansatz was confirmed by DFT calculations [59]. Note that this approach is only useful when the spin-crossover-induced structural change is mainly due to a uniform change of the metal-ligand bond distances. A notable exception where the structural change is more complicated is for the  $[\text{Fe}(\text{tpy})_2]^{2+}$  complex which, like the  $[\text{Fe}(\text{bpy})_2]^{2+}$  complex, has polypyridine ligands [67].

In fact, though the spin-state energetics are similar in these two complexes, different values of  $k_{\text{HL}}(T \rightarrow 0 \text{ K})$  have been measured in the range  $10^{-6}$ - $10^7 \text{ s}^{-1}$  in different environments. For  $[\text{Fe}(\text{bpy})_3]^{2+}$  doped in isostructural host crystals  $[\text{M}(\text{bpy})_3](\text{PF}_6)_2$  ( $\text{M} = \text{Co}, \text{Zn}, \text{Mn}, \text{Cd}$ ),  $k_{\text{HL}}(T \rightarrow 0 \text{ K})$  increases monotonically from  $\sim 10^3$  to  $\sim 10^6 \text{ s}^{-1}$  with a corresponding shrinking of the unit cell which, over the host series, is  $\sim 2\%$  [67]. This example allows to emphasize the usefulness of the concept of “chemical pressure” for explaining the influence of the environment on the electronic properties of spin-crossover and related complexes. However, this does not give us a detailed picture of the host-guest interactions which are at play. A deeper analysis of these interactions is, in fact, possible via DFT calculations, such as those which have recently been used to study  $[\text{Fe}(\text{bpy})_3]^{2+}$  included in a zeolite Y via the supermolecular model of  $[\text{Fe}(\text{bpy})_3]^{2+}@\text{Y}$  shown in Fig. 4 [98].

Zeolites provide a well-defined rigid three-dimensional network with a diversity of cavities of different sizes and shapes. Thus the environment of the complex may be controlled by choosing the cavities in which the complex is included. The zeolite Y supercage has a diameter of about 13 Å and an opening of  $\approx 7.4 \text{ Å}$  which allows the encapsulation of complexes of the same diameter *via in situ* synthesis. This is the case of *tris*(2,2'-bipyridine)

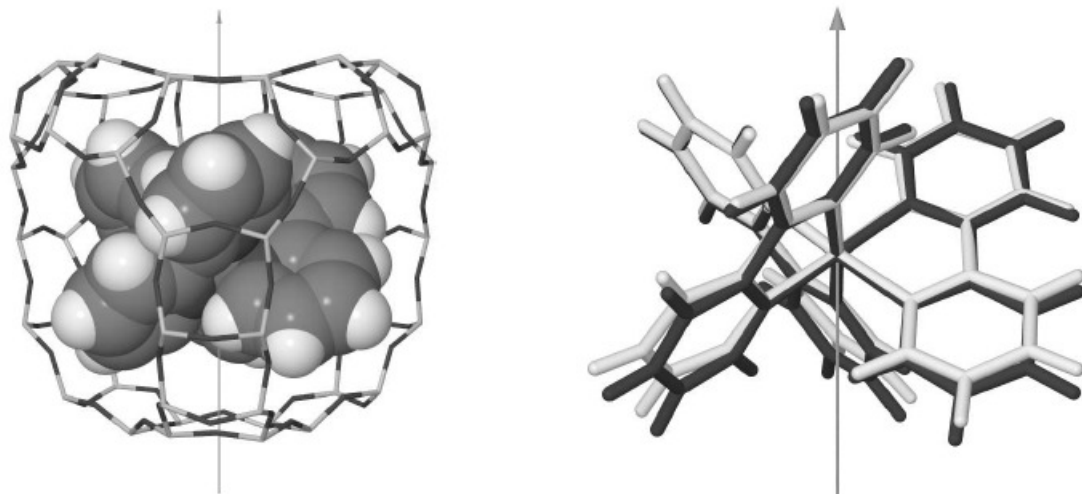


Figure 4: Left:  $C_3$  supermolecular model of the inclusion compound  $[\text{Fe}(\text{bpy})_3]^{2+}@\text{Y}$ : the model is composed of the complex along with the surrounding atoms of oxygen and silicon which define the supercage. Note that the silicon atom valence is saturated by hydrogen atoms which are not shown for graphic simplicity. Right: Comparison of the LS gas phase (black) and zeolite-embedded (white)  $[\text{Fe}(\text{bpy})_3]^{2+}$  geometries. The cage effect gives a slight contraction and distortion of the geometry of the complex. Figure reproduced with permission from Ref. [98].

complexes. For  $[\text{Fe}(\text{bpy})_3]^{2+}@\text{Y}$ , the formation of the LS complex may be characterized by X-ray diffraction combined possibly with infrared spectroscopy, UV-visible reflection spectroscopy or solid state NMR [99–102].

Mössbauer absorption spectroscopy of  $^{57}\text{Fe}$  may also be used [99, 103]. For iron spin crossover compounds, Mössbauer spectroscopy provides information about oxidation states, coordination of the central iron atom, and the distortion of the complexes from octahedral symmetry. The  $C_3$  symmetry model shown in Fig. 4 has been proposed on the basis of experimental data. DFT calculations have been carried out for this 229 atom structure for both the HS and LS states [98]. In particular, the molecular structures of  $[\text{Fe}(\text{bpy})_3]^{2+}$  and of  $[\text{Fe}(\text{bpy})_3]^{2+}@\text{Y}$  were optimized in their two spin states using various GGA and hybrid functionals. The optimized HS and LS structures obtained using different density functionals are very similar. A careful look shows that caging in the zeolite results in a slight shrinking and a slight distortion of the  $[\text{Fe}(\text{bpy})_3]^{2+}$  structure (Fig. 4). Caging has more effect on the HS state than on the LS state because the LS state is spatially more compact than is the HS state. The  $^{57}\text{Fe}$  quadrupolar splitting  $\Delta E_Q$  provides one measure of the distortion of the complex.  $\Delta E_Q$  has thus been calculated for the  $[\text{Fe}(\text{bpy})_3]^{2+}$  complex in isolation and caged within the zeolite, and it has been found to be correlated with the predicted degree

Table 4: Calculated HS-LS energy differences  $\Delta E_{\text{HL}}$  ( $\text{cm}^{-1}$ ) in  $[\text{Fe}(\text{bpy})_3]^{2+}$  and in  $[\text{Fe}(\text{bpy})_3]^{2+}@\text{Y}$ , variation  $\Delta(\Delta E_{\text{HL}})$  of  $\Delta E_{\text{HL}}$  after being caged in the zeolite, and decomposition of  $\Delta(\Delta E_{\text{HL}})$  into its geometric part  $\Delta E_{\text{HL}}^{\text{dist}}$  and the host-guest interaction energy  $\Delta E_{\text{HL}}^{\text{int}}$ . The HS state considered here is the trigonal  ${}^5\text{A}$  state of the ligand field  ${}^5\text{T}_{2g}$  state. Nevertheless both trigonal  ${}^5\text{E}$  and  ${}^5\text{A}$  states are close in energy. Adapted from Ref. [98]

	PBE	B3LYP*	HCTH	O3LYP	OLYP
HS-LS energy difference $\Delta E_{\text{HL}}$					
$[\text{Fe}(\text{bpy})_3]^{2+}$	+10087	+3849	+141	-811	+3660
$[\text{Fe}(\text{bpy})_3]^{2+}@\text{Y}$	+12004	+5925	+2687	+1941	+6594
$\Delta(\Delta E_{\text{HL}}) = \Delta E_{\text{HL}}[\text{Y}] - \Delta E_{\text{HL}}[\emptyset]$					
	+1917	+2076	+2546	+2752	+2934
$\Delta(\Delta E_{\text{HL}}) = \Delta E_{\text{HL}}^{\text{int}} + \Delta E_{\text{HL}}^{\text{dist}}$					
$\Delta E_{\text{HL}}^{\text{int}}$	+1246	+1267	+1621	+1286	+1331
$\Delta E_{\text{HL}}^{\text{dist}}$	+671	+809	+925	+1466	+1593

of distortion of the HS and LS complexes as measured by the ratio  $\xi$  of Fe-N distances (see Ref. [98]).<sup>2</sup> Moreover the  $\Delta E_Q$  values calculated for for LS  $[\text{Fe}(\text{bpy})_3]^{2+}@\text{Y}$  are in good (even very good) agreement with the experimental value  $\Delta E_Q \approx 0.32 \text{ mm.s}^{-1}$  of Vankó *et al.*[103] This emphasizes the pertinence of the model for  $[\text{Fe}(\text{bpy})_3]^{2+}@\text{Y}$ .

DFT provides a very satisfying description of  $[\text{Fe}(\text{bpy})_3]^{2+}@\text{Y}$  structures and Mössbauer properties in the HS and LS states. However, as may be anticipated (Sec. 3), and as shown in the data in Table 4, evaluating the HS and LS energies of  $[\text{Fe}(\text{bpy})_3]^{2+}@\text{Y}$  remains a difficult problem for DFT. In fact, the calculated energy difference  $\Delta E_{\text{HL}}[\text{Y}]$  varies between +1941 and +12004  $\text{cm}^{-1}$  depending upon the functional used. Nevertheless all the functionals predict that caging destabilizes the HS state more than the LS state. Furthermore the values found for the variation  $\Delta(\Delta E_{\text{HL}})$  of  $\Delta E_{\text{HL}}$  are very consistent with each other, all being between +1917 and +2934  $\text{cm}^{-1}$ , which is within our expected accuracy limitations for transition metal complexes. As we shall see below, the functionals used here permit a quantitative description of caging effects. The best estimation of  $\Delta(\Delta E_{\text{HL}})$  is thus [98],

$$\begin{aligned} \Delta(\Delta E_{\text{HL}}) &= \Delta E_{\text{HL}}[\text{Y}] - \Delta E_{\text{HL}}[\emptyset] \\ &= +2500 \pm 1000 \text{ cm}^{-1}. \end{aligned} \quad (4)$$

The notation  $X[\emptyset]$  and  $X[\text{Y}]$  stand for the values of  $X$  evaluated for the isolated  $[\text{Fe}(\text{bpy})_3]^{2+}$

<sup>2</sup>In the gas phase, the complex has the symmetry  $D_3$  and all the Fe-N distances are identical:  $\xi = 1$ .  $[\text{Fe}(\text{bpy})_3]^{2+}@\text{Y}$  has  $C_3$  symmetry with two different Fe-N distances whose ratio  $\xi < 1$  depends upon the degree of distortion of the complex.

and for the caged  $[\text{Fe}(\text{bpy})_3]^{2+}@\text{Y}$  respectively. In order to analyse the influence of host-guest interactions on spin-state energies,  $\Delta(\Delta E_{\text{HL}})$  has been decomposed into two contributions:  $\Delta E_{\text{HL}}^{\text{dist}}$  and  $\Delta E_{\text{HL}}^{\text{int}}$ . The first is the HS-LS energy difference:  $\Delta E_{\text{HL}}^{\text{dist}} = E_{\text{HS}}^{\text{dist}} - E_{\text{LS}}^{\text{dist}}$ , where  $E_{\Gamma}^{\text{dist}}$  ( $\Gamma = \text{HS}, \text{LS}$ ) is the energy needed to deform in the spin state  $\Gamma$  the structures of the complex and the surrounding cage network from their dissociated and relaxed structures to those found in  $[\text{Fe}(\text{bpy})_3]^{2+}@\text{Y}$ . The second is the variation of guest-host interaction energy  $E^{\text{int}}$  induced by the  $\text{LS} \rightarrow \text{HS}$  change of state:  $\Delta E_{\text{HL}}^{\text{int}} = E_{\text{HS}}^{\text{int}} - E_{\text{LS}}^{\text{int}}$ .

Table 4 shows that the value of  $\Delta E_{\text{HL}}^{\text{int}}$  is relatively independent of the functional used ( $\Delta E_{\text{HL}}^{\text{int}} \approx +1300 \text{ cm}^{-1}$ , contrary to the case for  $\Delta E_{\text{HL}}^{\text{dist}}$ ). The variation in the values of  $\Delta E_{\text{HL}}^{\text{dist}}$  is thus responsible for the spread of values in  $\Delta(\Delta E_{\text{HL}})$ . This can be traced back to the influence of the functional on the description of the complex caged in the zeolite Y supercage [98].  $\Delta E_{\text{HL}}^{\text{dist}} > 0$  because the distortional energy is greater in the HS than in the LS state. Also  $\Delta E_{\text{HL}}^{\text{int}} > 0$  as the host-guest interactions become less stabilizing after the  $\text{LS} \rightarrow \text{HS}$  transition. The instantaneous interaction energy  $E^{\text{int}}$  between the two fragments may be further decomposed [76, 104] as,

$$E^{\text{int}} = E^{\text{elstat}} + E^{\text{Pauli}} + E^{\text{orb}}. \quad (5)$$

$E^{\text{elstat}}$  is the classical electrostatic energy between the unperturbed charge distributions of the host and guest;  $E^{\text{Pauli}}$  is the Pauli repulsion responsible for steric repulsions; and  $E^{\text{orb}}$  is the orbital energy contribution, i.e., the energy obtained upon relaxation of the electron density. More precisely, the Pauli repulsion is the change in the energy in going from a simple superposition of the unrelaxed density of the two fragments to the wavefunction of the two fragments together obtained by antisymmetrization and normalization of the product of the fragment wavefunctions. Table 5 shows the results obtained by this analysis of the host-guest interactions in  $[\text{Fe}(\text{bpy})_3]^{2+}@\text{Y}$ . Notice that the interactions are binding in the two spin states ( $E_{\Gamma}^{\text{int}} < 0$ ) and that the binding is more electrostatic than covalent ( $E_{\Gamma}^{\text{elstat}} < E_{\Gamma}^{\text{orb}} < 0$ ;  $\Gamma = \text{HS}, \text{LS}$ ). In going from the LS to the HS state, the change in the interaction energy is  $\Delta E_{\text{HL}}^{\text{int}} = +1248 \text{ cm}^{-1}$ , in very good agreement with the value given in Tab. 4. The largest contribution to  $\Delta E_{\text{HL}}^{\text{int}}$  comes from the Pauli repulsion, which is intuitively consistent with the increase in the size of the complex in going from the LS to the HS state. However  $\Delta E_{\text{HL}}^{\text{Pauli}}$  only represents about 53% of  $\Delta E_{\text{HL}}^{\text{int}}$ : The electrostatic and orbital interaction energies are less stabilizing and contribute to 47% of  $\Delta E_{\text{HL}}^{\text{int}}$ . This is more difficult to rationalize based upon chemical intuition alone.

Table 5: Analysis of the host-guest interactions in  $[\text{Fe}(\text{bpy})_3]^{2+}$  in the HS and LS states (energies in  $\text{cm}^{-1}$  for the OLYP functional) [98]

	$E_{\Gamma}^{\text{elstat}}$	$E_{\Gamma}^{\text{Pauli}}$	$E_{\Gamma}^{\text{orb}}$	$E_{\Gamma}^{\text{int}}$
$\Gamma = \text{LS}$	-15558	+17442	-12158	-10274
$\Gamma = \text{HS}$	-15251	+18099	-11874	-9026
	$\Delta E_{\Gamma}^{\text{elstat}}$	$\Delta E_{\Gamma}^{\text{Pauli}}$	$\Delta E_{\Gamma}^{\text{orb}}$	$\Delta E_{\Gamma}^{\text{int}}$
	+307	+657	+284	+1248

In fact, for a given geometry  $[\text{M}(\text{bpy})_3]^{2+}@\text{Y}$  where  $\text{M}^{2+}$  is a doubly-charged transition metal cation, the host-guest interaction energies are independent of the metal cation spin state. It follows that the host-guest interactions in the  $[\text{M}(\text{bpy})_3]^{2+}@\text{Y}$  inclusion compound are *closed-shell interactions between the first coordination sphere of the complex and the second coordination sphere constituted by atoms of the surrounding zeolite, polarized by the doubly-charged cation* [98]. The good performance of most modern functionals for the description of interactions between closed shells explains the good performance obtained. As concerns spin-state energies, the best estimate of  $\Delta E_{\text{HL}}[\emptyset]$  obtained from CASPT2 calculations is  $3700 \pm 1000 \text{ cm}^{-1}$  [17, 18]. Combining this result and that of Eq. (4) gives

$$\Delta E_{\text{HL}}[\text{Y}] = 6200 \pm 1500 \text{ cm}^{-1},$$

as the best estimate of the energy difference between the two spin states in  $[\text{Fe}(\text{bpy})_3]^{2+}@\text{Y}$  and a difference of zero point energies of  $\Delta E_{\text{HL}}^{\circ}[\text{Y}] \approx 5400 \text{ cm}^{-1}$  [98]. In the theory of HS  $\rightarrow$  LS relaxation presented above [67], the value of  $\Delta E_{\text{HL}}^{\circ}[\text{Y}]$  corresponds to a lifetime  $\tau_{\text{HS}} = 1/k_{\text{HL}}(T \rightarrow 0 \text{ K})$  of the HS state of 10 ns at most. This agrees with the limit  $\tau_{\text{HS}}[\text{Y}] \leq 60 \text{ ns}$  deduced from Mössbauer emission spectroscopy [105].

The study of  $[\text{Fe}(\text{bpy})_3]^{2+}@\text{Y}$  shows that DFT allows environmental effects to be taken into account in an efficient and reliable fashion. The DFT calculations have indeed allowed the quantification of the effect of caging on the structure of the complex in the HS and LS states, the determination of the relative energies of the spin states, and finally a detailed analysis of guest-host interactions. Furthermore periodic DFT studies offer interesting possibilities for a deeper understanding of the effects of crystal packing and of counter ions in the solid state. Such studies can also help gain insights into how sorption of guest molecules modulate the spin state of spin-crossover complexes encaged in porous metal-organic frameworks, a mechanism developed for the design of a novel spin-crossover porous hybrid architecture for potential sensing applications [106].

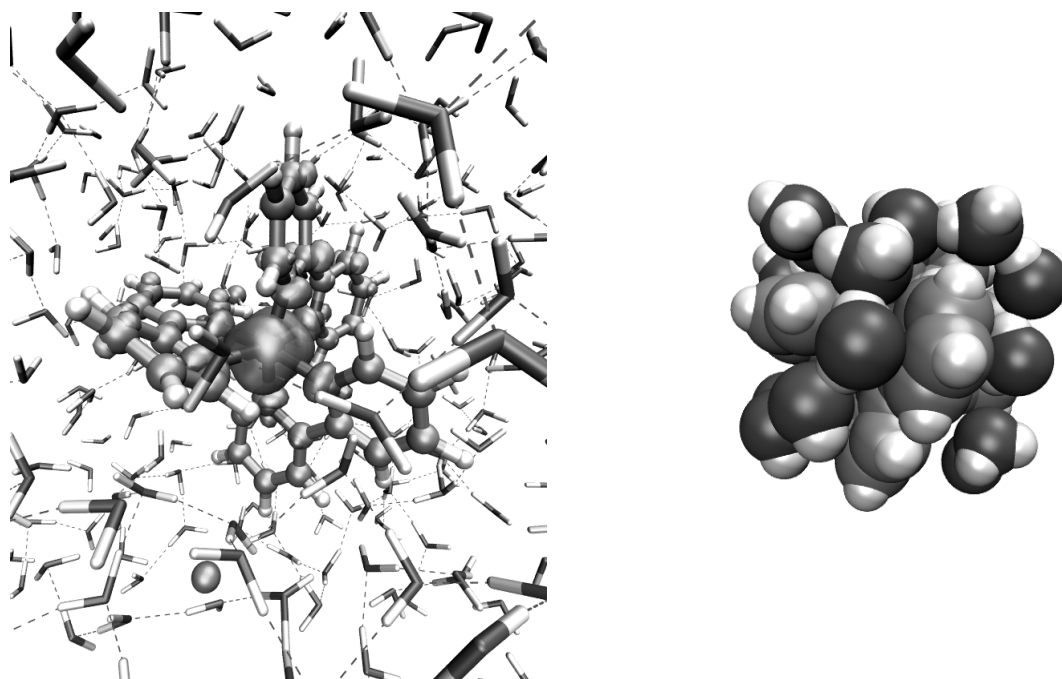


Figure 5: Car-Parrinello molecular dynamics study of  $[\text{Fe}(\text{bpy})_3](\text{Cl})_2$  at 300 K in the LS and HS states Ref. [107]. Left: snapshot from the HS  $[\text{Fe}(\text{bpy})_3]^{2+}$  trajectory showing  $[\text{Fe}(\text{bpy})_3]^{2+}$ , a  $\text{Cl}^-$  anion, water molecules, and the spin-density on the iron. Right: snapshot from the LS trajectory showing that the first solvation shell around the complex is made up of water molecules inserted into the spaces between the ligands. Figure adapted from Ref. [107].

Similarly the study of Fe(II) complexes in solution by molecular dynamics simulations allowed to progress in the comprehension of the spin-state dependence of their structural and vibrational properties, evidencing the strong interpenetration between their coordination sphere and their hydration shell [107–109]. This study has been initiated to complement experiment. The mechanism of the photoinduced LS  $\rightarrow$  HS change of states is indeed extensively investigated for spin-crossover and LS Fe(II) complexes in solution using ultrafast X-ray, [110–128] UV-vis [129–135] and vibrational [131, 136, 137] spectroscopies. Much attention is paid to the prototypical  $[\text{Fe}(\text{bpy})_3]^{2+}$  complex in water (Fig. 5), which has been the subject of several molecular dynamics studies [107, 138–141]. Combining forefront spectroscopy studies and state-of-the-art molecular dynamics simulations really proved to be a promising approach for gaining insights into the mechanism of the photoinduced LS  $\rightarrow$  HS change of states. This recently allowed visualizing the coordination spheres of photo-excited aqueous  $[\text{Fe}(\text{bpy})_3]^{2+}$  [142].

## 6. The Future

The last two decades have seen major progresses in the modelling of spin-crossover complexes. This may be better apprehended by recalling the three Pauling points presented in the beginning of the chapter. Thus, it must first be emphasized that LFT (the first point) is still very important in the sense that it is inextricably linked to the way experimentalists think about transition metal complexes. Advances beyond LFT have come from the concerted effort of several groups which have converged to establish the second Pauling point (DFT and TD-DFT.) Not only does DFT perform well for the calculation of geometries, vibrational frequencies, and other properties of LS and HS complexes, but DFT is increasingly able to give information about the relative energies of the different spin states. This is partly due to the development of specific procedures, including the reparameterization of hybrid functionals, the discovery of useful functionals on the lower rungs of Jacob's ladder, and the discovery of functional-independent invariants which can allow calculations to be less dependent on the choice of functional. Progress also concerns the third Pauling point and a synergy has begun to emerge between the second and third Pauling points. Thus coupled-cluster calculations are now able to validate DFT results for the relative energies of different spin states for small- to medium-sized complexes. In the future, the authors expect to see increasing number of coupled-cluster and large-active-space CASSCF/CASPT2 calculations on spin-crossover complexes. Nevertheless DFT and TD-DFT will continue to be their main tools, particularly for the study of large systems and especially when it is necessary to take into account environmental effects and/or photodynamics. This chapter has presented some of the work of the authors going in this direction.

## References

- [1] P. Gütllich, H. A. Goodwin (Eds.), *Spin Crossover in Transition Metal Compounds I-III*, Vol. 233-235 of *Top. Curr. Chem.*, Springer-Verlag, Heidelberg, 2004.
- [2] J. H. Askew, H. J. Shepherd, Mechanochemical synthesis of cooperative spin crossover materials, *Chem. Commun.* 54 (2018).
- [3] G. E. P. Box, N. R. Draper, *Empirical Model-Building and Response Surfaces*, Wiley, 1987, p. 424.
- [4] In an interview at the University of Pisa on 9 September 1993, Roy McWeeny said, "There There is one anecdote here that might be of interest. At one of the first meetings I ever went to, I think it was in '57, both Pauling and Mulliken were present. It was a meeting arranged by Löwdin in Sweden. And at that meeting the phrase was coined : 'The Pauling Point'. That is the point at which — when you get oscillating results — you stop. Because Pauling always right was, he stopped at the right point!" See <http://www.quantum-chemistry-history.com/McWee1.htm> (Last accessed: July 6, 2020).

- [5] B. N. Figgis, M. A. Hitchman, *Ligand Field Theory and Its Applications*, Wiley-VCH, New York, 2000.
- [6] B. O. Roos, P. R. Taylor, P. E. M. Siegbahn, A complete active space SCF method (CASSCF) using a density matrix formulated super-CI approach, *Chem. Phys.* 48 (1980) 157–173.
- [7] R. J. Bartlett, M. Musiał, Coupled-cluster theory in quantum chemistry, *Rev. Mod. Phys.* 79 (2007) 291–352.
- [8] C. Hättig, Electronic structure: Hartree-Fock and correlation methods, in: J. Grotendorst, N. Atig, S. Blügel, D. Marx (Eds.), *Multiscale Simulation Methods in Molecular Sciences*, NIC Series, Forschungszentrum Jülich, Germany, 2009, pp. 77–120.
- [9] L. M. Lawson Daku, F. Aquilante, T. W. Robinson, A. Hauser, Accurate Spin-State Energetics of Transition Metal Complexes: I. CCSD(T), CASPT2 and DFT Study of  $[M(\text{NCH})_6]^{2+}$  ( $M = \text{Fe}, \text{Co}$ ), *J. Chem. Theory Comput.* 8 (2012) 4216–4231.
- [10] M. Radoń, Spin-State Energetics of Heme-Related Models from DFT and Coupled Cluster Calculations, *J. Chem. Theory Comput.* 10 (6) (2014) 2306–2321. doi:10.1021/ct500103h.
- [11] K. Andersson, P.-Å. Malmqvist, B. O. Roos, A. J. Sadlej, K. Wolinski, Second-order perturbation theory with a CASSCF reference function, *J. Phys. Chem.* 94 (1990) 5483–5488.
- [12] K. Andersson, P.-Å. Malmqvist, B. O. Roos, Second-order perturbation theory with a complete active space self-consistent field reference function, *J. Chem. Phys.* 96 (1992) 1218–1226.
- [13] F. Neese, A spectroscopy oriented configuration interaction procedure, *J. Chem. Phys.* 119 (2003) 9428–9443.
- [14] J. Miralles, O. Castell, R. Caballol, J.-P. Malrieu, Specific CI calculation of energy differences: Transition energies and bond energies, *Chem. Phys.* 172 (1993) 33–43.
- [15] J. Miralles, J.-P. Daudey, R. Caballol, Variational calculation of small energy differences — The singlet-triplet gap in  $[\text{Cu}_2\text{Cl}_6]^{2-}$ , *Chem. Phys. Lett.* 198 (1992) 555–562.
- [16] H. Bolvin,  $d \rightarrow d$  spectrum and high-spin/low-spin competition in  $d^6$  octahedral coordination compounds: *Ab initio* study of potential energy curves, *J. Phys. Chem. A* 102 (1998) 7525–7534.
- [17] K. Pierloot, S. Vancoillie, Relative energy of the high- $(^5T_{2g})$  and low- $(^1A_{1g})$  spin states of  $[\text{Fe}(\text{H}_2\text{O})_6]^{2+}$ ,  $[\text{Fe}(\text{NH}_3)_6]^{2+}$ , and  $[\text{Fe}(\text{bpy})_3]^{2+}$ : CASPT2 versus density functional theory, *J. Chem. Phys.* 125 (2006) 124303.
- [18] K. Pierloot, S. Vancoillie, Relative energy of the high- $(^5T_{2g})$  and low- $(^1A_{1g})$  spin states of the ferrous complexes  $[\text{Fe}(\text{L})(\text{NHS}_4)]$ : CASPT2 versus density functional theory, *J. Chem. Phys.* 128 (2008) 034104.
- [19] M. Kepenekian, V. Robert, B. Le Guennic, C. de Graaf, Energetics of  $[\text{Fe}(\text{NCH})_6]^{2+}$  via CASPT2 calculations: A spin-crossover perspective, *J. Comput. Chem.* 30 (2009) 2327–2333.
- [20] M. Kepenekian, V. Robert, B. Le Guennic, What zeroth-order Hamiltonian for CASPT2 adiabatic energetics for  $\text{Fe}(\text{II})\text{N}_6$  architectures?, *J. Chem. Phys.* 131 (2009) 114702.
- [21] Q. M. Phung, M. Feldt, J. N. Harvey, K. Pierloot, Toward Highly Accurate Spin State Energetics in First-Row Transition Metal Complexes: A Combined CASPT2/CC Approach, *J. Chem. Theory Comput.* 14 (5) (2018) 2446–2455. doi:10.1021/acs.jctc.8b00057.
- [22] G. Li Manni, D. Kats, D. P. Tew, A. Alavi, Role of valence and semicore electron correlation on spin gaps in  $\text{Fe}(\text{II})$ -porphyrins, *J. Chem. Theory Comput.* 15 (3) (2019) 1492–1497, pMID: 30681852.

doi:10.1021/acs.jctc.8b01277.

URL <https://doi.org/10.1021/acs.jctc.8b01277>

- [23] L. H. Thomas, The calculation of atomic fields, *Proc. Cambridge Phil. Soc.* 23 (1927) 542–548.
- [24] E. Fermi, Un Metodo Statistico per la Determinazione di alcune Priorieta dell’Atome, *Rend. Accad. Naz. Lincei* 6 (1927) 602–607.
- [25] P. A. M. Dirac, Note on exchange phenomena in the Thomas atom, *Proc. Cambridge Phil. Soc.* 26 (1930) 376–385.
- [26] J. C. Slater, *Quantum Theory of Molecules and Solids*, Vol. 4 of International Series in Pure and Applied Physics, McGraw-Hill, 1974.
- [27] P. Hohenberg, W. Kohn, Inhomogeneous electron gas, *Phys. Rev.* 136 (1964) B864–B871.
- [28] M. Levy, Universal variational functionals of electron densities, first-order density matrices, and natural spin-orbitals and solution of the  $v$ -representability problem, *Proc. Natl. Acad. Sci.* 76 (1979) 6062–6065.
- [29] W. Kohn, L. J. Sham, Self-consistent equations including exchange and correlation effects, *Phys. Rev.* 140 (1965) A1133–A1138.
- [30] J. P. Perdew, K. Schmidt, Jacob’s ladder of density functional approximations for the exchange-correlation energy, in: V. E. V. Doren, K. V. Alseoy, P. Geerlings (Eds.), *Density Functional Theory and Its Applications to Materials*, American Institute of Physics, Melville, New York, 2001, p. 1.
- [31] J. P. Perdew, A. Ruzsinsky, L. A. Constantin, J. Sun, G. I. Csonka, Some fundamental issues in ground-state density functional theory: A guide for the perplexed, *J. Chem. Theory Comput.* 5 (2009) 902.
- [32] W. Koch, M. C. Holthausen, *A Chemist’s Guide to Density Functional Theory*, Wiley-VCH, New York, 2000.
- [33] R. G. Parr, W. Yang, *Density-Functional Theory of Atoms and Molecules*, Oxford University Press, New York, 1989.
- [34] R. M. Dreizler, E. K. U. Gross, *Density Functional Theory, An Approach to the Quantum Many-Body Problem*, Springer-Verlag, New York, 1990.
- [35] M. E. Casida, Review: Time-dependent density-functional theory for molecules and molecular solids, *J. Molec. Struct. (Theochem)* 914 (2009) 3.
- [36] J. P. Perdew, L. A. Constantin, Laplacian-level density functionals for the kinetic energy density and exchange-correlation energy, *Phys. Rev. B* 75 (2007) 155109.
- [37] A. Görling, Proper treatment of symmetries and excited states in a computationally tractable Kohn-Sham method, *Phys. Rev. Lett.* 85 (2000) 4229–4232.
- [38] A. Görling, Orbital- and state-dependent functionals in density-functional theory, *J. Chem. Phys.* 123 (2005) 062203.
- [39] I. G. Kaplan, Problems in DFT with the total spin and degenerate states, *Int. J. Quantum Chem.* 107 (2007) 2595–2603.
- [40] E. Runge, E. K. U. Gross, Density-functional theory for time-dependent systems, *Phys. Rev. Lett.* 52 (1984) 997–1000.
- [41] M. E. Casida, Time-dependent density functional response theory for molecules, in: D. P. Chong (Ed.), *Recent Advances in Density Functional Methods. Part I*, Vol. 1 of *Recent Advances in Computational*

- Chemistry, World Scientific, Singapore, 1995, pp. 155–192.
- [42] R. van Leeuwen, Key concepts in time-dependent density-functional theory, *Int. J. Mod. Phys. B* 15 (2001) 1969–2023.
- [43] C. Daniel, Electronic spectroscopy and photoreactivity in transition metal complexes, *Coordination Chem. Rev.* 238-239 (2003) 141.
- [44] M. A. L. Marques, E. K. U. Gross, Time-dependent density-functional theory, *Annu. Rev. Phys. Chem.* 55 (2004) 427.
- [45] A. Dreuw, M. Head-Gordon, Single-reference *ab initio* methods for the calculation of excited states of large molecules, *Chem. Rev.* 105 (2005) 4009.
- [46] G. D. Mahan, K. R. Subbaswamy, *Local Density Theory of Polarizability*, Plenum, New York, 1990.
- [47] M. A. L. Marques, C. Ullrich, F. Nogueira, A. Rubio, E. K. U. Gross (Eds.), *Time-Dependent Density-Functional Theory*, Vol. 706 of *Lecture Notes in Physics*, Springer, Berlin, 2006.
- [48] M. Head-Gordon, E. Artacho, Chemistry on the computer, *Physics Today* 61 (4) (2008) 58.
- [49] A. D. Becke, Density-functional exchange-energy approximation with correct asymptotic behavior, *Phys. Rev. B* 38 (1988) 3098.
- [50] J. P. Perdew, Density-functional approximation for the correlation energy of the inhomogeneous electron gas, *Phys. Rev. B* 33 (1986) 8822.
- [51] C. Lee, W. Yang, R. G. Parr, Development of the Colle-Salvetti correlation energy formula into a functional of the electron density, *Phys. Rev. B* 38 (1988) 3098.
- [52] J. P. Perdew, K. Burke, Y. Wang, Generalized gradient approximation for the exchange-correlation hole of a many-electron system, *Phys. Rev. B* 54 (1996) 16533, erratum, *ibid* 57, 14999 (1988).
- [53] J. P. Perdew, K. Burke, M. Ernzerhof, Generalized gradient approximation made simple, *Phys. Rev. Lett.* 77 (1996) 3865, erratum, *ibid* 78, 1386 (1997).
- [54] B. Hammer, L. B. Hansen, J. K. Nørskov, Improved adsorption energetics within density-functional theory using revised Perdew-Burke-Ernzerhof functionals, *Phys. Rev. B* 59 (1999) 7413.
- [55] S. H. Vosko, L. Wilk, M. Nusair, Accurate spin-dependent electron liquid correlation energies for local spin density calculations: A critical analysis., *Can. J. Phys.* 58 (1980) 1200.
- [56] A. Becke, Density-functional thermochemistry. III. The role of exact exchange, *J. Chem. Phys.* 98 (1993) 5648.
- [57] A. Fouqueau, S. Mer, M. E. Casida, L. M. Lawson Daku, A. Hauser, T. Mineva, F. Neese, Comparison of density functionals for energy and structural differences between the high [ ${}^5T_{2g} : (t_{2g})^4(e_g)^2$ ] and low [ ${}^1A_{1g} : (t_{2g})^6(e_g)^0$ ] spin states of the hexaquoferrous cation,  $[\text{Fe}(\text{H}_2\text{O})_6]^{2+}$ , *J. Chem. Phys.* 120 (2004) 9473.
- [58] A. Fouqueau, M. E. Casida, L. M. Lawson Daku, A. Hauser, F. Neese, Comparison of density functionals for energy and structural differences between the high [ ${}^5T_{2g} : (t_{2g})^4(e_g)^2$ ] and low [ ${}^1A_{1g} : (t_{2g})^6(e_g)^0$ ] spin states of iron(II) coordination compounds: II. More functionals and the hexaminoferrous cation,  $[\text{Fe}(\text{NH}_3)_6]^{2+}$ , *J. Chem. Phys.* 122 (2005) 044110.
- [59] L. M. Lawson Daku, A. Vargas, A. Hauser, A. Fouqueau, M. E. Casida, Assessment of Density Functionals for the High-Spin/Low-Spin Energy Difference in the Low-Spin Iron(II) Tris(2,2'-bipyridine) Complex, *ChemPhysChem* 6 (2005) 1393–1410.
- [60] F. A. Hamprecht, A. J. Cohen, D. J. Tozer, N. C. Handy, Development and assessment of new

- exchange-correlation functionals, *J. Chem. Phys.* 109 (1998) 6264.
- [61] T. V. Voorhis, G. E. Scuseria, A novel form for the exchange-correlation energy functional, *J. Chem. Phys.* 109 (1998) 400.
- [62] C. Adamo, V. Barone, Toward reliable density functional methods without adjustable parameters: The PBE0 model, *J. Chem. Phys.* 110 (1999) 6158.
- [63] N. C. Handy, A. J. Cohen, Left-right correlation energy, *Mol. Phys.* 99 (2001) 403.
- [64] O. Salomon, M. Reiher, B. A. Hess, Assertion and validation of the performance of the B3LYP\* functional for the first transition metal row and the G2 test set, *J. Chem. Phys.* 117 (2002) 4729–4737.
- [65] G. Ganzenmüller, N. Berkaïne, A. Fouqueau, M. E. Casida, M. Reiher, Comparison of density functionals for differences between the high ( ${}^5T_{2g}$ ) and low ( ${}^1A_{1g}$ ) spin states of Iron(II) coordination compounds: IV. Results for the ferrous complexes [Fe(L)(‘NHS<sub>4</sub>’)], *J. Chem. Phys.* 122 (2005) 234321.
- [66] M. Swart, Accurate spin-state energetics for iron complexes, *J. Chem. Theory Comput.* 4 (2007) 2057.
- [67] A. Hauser, C. Enachescu, M. Lawson Daku, A. Vargas, N. Amstutz, Review. Low-temperature lifetimes of metastable high-spin states in spin-crossover and in low-spin compounds: The rule and exceptions to the rule, *Coord. Chem. Rev.* 250 (2006) 1642–1652.
- [68] M. Reiher, Theoretical study of the Fe(phen)<sub>2</sub>(NCS)<sub>2</sub> spin-crossover complex with reparametrized density functionals, *Inorg. Chem.* 41 (2002) 6928–6935.
- [69] S. Zein, S. A. Borshch, P. Fleurat-Lessard, M. E. Casida, H. Chermette, Assessment of the exchange-correlation functionals for the physical description of spin transition phenomena by DFT methods: All the same?, *J. Chem. Phys.* 126 (2007) 014105.
- [70] A. Vargas, I. Krivokapic, A. Hauser, L. M. Lawson Daku, Towards accurate estimates of the spin-state energetics of spin-crossover complexes within density functional theory: a comparative case study of cobalt(II) complexes, *Phys. Chem. Chem. Phys.* 15 (2013) 3752–3763. doi:10.1039/C3CP44336A.
- [71] M. Grätzel, Photoelectrochemical cells, *Nature* 414 (2001) 338.
- [72] E. K. U. Gross, W. Kohn, Time-dependent density functional theory, *Adv. Quant. Chem.* 21 (1990) 255.
- [73] E. K. U. Gross, C. A. Ullrich, U. J. Gossmann, Density functional theory of time-dependent systems, in: E. K. U. Gross, R. M. Dreizler (Eds.), *Density Functional Theory*, Plenum, New York, 1994, pp. 149–171.
- [74] M. E. Casida, Time-dependent density functional response theory of molecular systems: Theory, computational methods, and functionals, in: J. M. Seminario (Ed.), *Recent Developments and Applications of Modern Density Functional Theory*, Elsevier, Elsevier, Amsterdam, 1996, p. 391.
- [75] K. Burke, E. K. U. Gross, A guided tour of time-dependent density functional theory, in: D. Joubert (Ed.), *Density Functionals: Theory and Applications*, Vol. 500 of Springer Lecture Notes in Physics, Springer, 1998, pp. 116–146.
- [76] G. te Velde, F. M. Bickelhaupt, E. J. Baerends, C. Fonseca, C. Guerra, S. J. A. van Gisbergen, J. G. Snijders, T. Ziegler, Chemistry with ADF, *J. Comput. Chem.* 22 (2001) 931.
- [77] M. E. Casida, Jacob’s ladder for time-dependent density-functional theory: Some rungs on the way to photochemical heaven, in: M. R. H. Hoffmann, K. G. Dyall (Eds.), *Accurate Description of Low-Lying Molecular States and Potential Energy Surfaces*, ACS Press, Washington, D.C., 2002, p. 199.
- [78] M. A. L. Marques, E. K. U. Gross, Time-dependent density functional theory, in: C. Fiolhais,

- F. Nogueira, M. A. L. Marques (Eds.), *A Primer in Density Functional Theory*, Vol. 620 of Springer Lecture Notes in Physics, Springer, 2003, pp. 144–184.
- [79] K. Burke, J. Werschnik, E. K. U. Gross, Time-dependent density functional theory: Past, present and future, *J. Chem. Phys.* 123 (2005) 062206.
- [80] A. Castro, M. A. L. Marques, H. Appel, M. Oliveira, C. A. Rozzi, X. Andrade, F. Lorenzen, E. K. U. Gross, A. Rubio, Octopus: a tool for the application of time-dependent density functional theory, *Physica Status Solidi* 243 (2006) 2465.
- [81] M. E. Casida, TDDFT for excited states, in: P. Sautet, R. A. van Santen (Eds.), *Computational Methods in Catalysis and Materials Science*, Wiley-VCH, Weinheim, Germany, 2008, p. 33.
- [82] A. Vargas, M. Zerara, E. Krausz, A. Hauser, L. M. Lawson Daku, Density-functional theory investigation of the geometric, energetic, and optical properties of the cobalt(II)tris(2,2'-bipyridine) complex in the high-spin and the Jahn-Teller active low-spin states, *J. Chem. Theory Comput.* 2 (2006) 1342–1359.
- [83] M. E. Casida, A. Ipatov, F. Cordova, Linear-response time-dependent density functional theory for open-shell molecules, in: M. A. L. Marques, C. Ullrich, F. Nogueira, A. Rubio, E. K. U. Gross (Eds.), *Time-Dependent Density-Functional Theory*, Vol. 706 of Lecture Notes in Physics, Springer, 2006, pp. 243–257.
- [84] A. Ipatov, F. Cordova, L. Joubert Doriol, M. E. Casida, Excited-state spin-contamination in time-dependent density-functional theory for molecules with open-shell ground states, *J. Molec. Struct. (Theochem)* 914 (2009) 60.
- [85] H. Myneni, M. E. Casida, On the calculation of  $\Delta\langle S^2 \rangle$  for electronic excitations in time-dependent density-functional theory, *Comput. Phys. Comm.* 213 (2017) 72.
- [86] B. E. Fleurinor, Courbes d'énergie potentielle des états excités de la molécule  $[\text{Fe}(\text{H}_2\text{O})_6]^{2+}$  par la méthode de la théorie fonctionnelle de la densité indépendante et dépendante du temps, rapport de stage en L2 Chimie, Université Joseph Fourier, 27 juin au 1 septembre 2006.
- [87] B. E. Fleurinor, *Courbes d'énergie potentielle des états excités de la molécule  $[\text{Fe}(\text{H}_2\text{O})_6]^{2+}$  par la méthode de la Théorie Fonctionnelle de la Densité Indépendante et Dépendante du temps*, Third year Bachelors project report in Chemistry, Joseph Fourier University 3-30 January 2007.
- [88] S. Bruneau, *Au delà de la théorie du champ de ligand avec la théorie de la fonctionnelle de la densité dépendante du temps : Contamination de spin et assignation des états pour les états électroniques du complexe hexaquofer(II)  $[\text{Fe}(\text{H}_2\text{O})_6]^{2+}$* , First year Masters report in Chemistry, Joseph Fourier University, 30 March - 26 June 2009.
- [89] L. J. Doriol, *Développement des méthodes d'études des états à couches ouvertes dans le cadre de la théorie de la fonctionnelle de la densité DFT dépendante du temps TDDFT*, Second year Masters report in Physical Chemistry, Joseph Fourier University, March-June 2009.
- [90] F. Cordova, L. Joubert Doriol, A. Ipatov, M. E. Casida, C. Filippi, A. Vela, Troubleshooting time-dependent density-functional theory for photochemical applications: Oxirane, *J. Chem. Phys.* 127 (2007) 164111.
- [91] E. Tapavicza, I. Tavernelli, U. Röthlisberger, Trajectory surface hopping within linear response time-dependent density-functional theory, *Phys. Rev. Lett.* 98 (2007) 023001.
- [92] R. Mirić, U. Werner, V. Bonačić-Koutecký, Nonadiabatic dynamics and simulation of time resolved

- photoelectron spectra within time-dependent density functional theory: Ultrafast photoswitching in benzylideneaniline, *J. Chem. Phys.* 129 (2008) 164118.
- [93] E. Tapavicza, I. Tavernelli, U. Rothlisberger, C. Filippi, M. E. Casida, Mixed time-dependent density-functional theory/classical trajectory surface hopping study of oxirane photochemistry, *J. Chem. Phys.* 129 (2008) 124108.
- [94] U. Werner, R. Mitrić, T. Suzuki, V. Bonačić-Koutecký, Nonadiabatic dynamics within the time dependent density functional theory: Ultrafast photodynamics in pyrazine, *Chem. Phys.* 349 (2008) 319.
- [95] M. Barbatti, J. Pitner, M. Pederzoli, R. M. U. Werner, V. Bonačić-Koutecký, H. Lischka, Non-adiabatic dynamics of pyrrole: Dependence of deactivation mechanisms on the excitation energy, *Chem. Phys.* 375 (2010) 26.
- [96] B. G. Levine, C. Ko, J. Quenneville, T. J. Martinez, Conical intersections and double excitations in time-dependent density functional theory, *Mol. Phys.* 104 (2006) 1039.
- [97] A. Hauser, Light-Induced Spin Crossover and the High-Spin→Low-Spin Relaxation, in: P. Gütllich, H. A. Goodwin (Eds.), *Spin Crossover in Transition Metal Compounds II*, Vol. 234 of *Top. Curr. Chem.*, Springer-Verlag, Heidelberg, 2004, pp. 155–198.
- [98] A. Vargas, A. Hauser, L. M. Lawson Daku, Influence of guest-host interactions on the structural, energetic, and Mössbauer spectroscopy properties of Iron(II)tris(2,2'-bipyridine) in the low-spin and high-spin states: A density-functional theory study of the zeolite-y embedded complex, *J. Chem. Theory Comput.* 5 (2009) 97–115.
- [99] W. H. Quayle, G. Peeters, G. L. De Roy, E. F. Vansant, J. H. Lunsford, Synthesis and Spectroscopic Properties of Divalent and Trivalent Tris(2,2'-dipyridine)iron Complexes in Zeolite Y, *Inorg. Chem.* 21 (1982) 2226.
- [100] Y. Umemura, Y. Minai, T. Tominaga, Evidence for Distortion in  $[\text{FeL}_3]^{2+}$  (L = en, amp, bpy, phen) in a Y-type Zeolite, *J. Chem. Soc. Chem. Commun.* (1993) 1822.
- [101] Y. Umemura, Y. Minai, T. Tominaga, Structural Distortion of 6-Coordinated Fe(II) Complexes in Zeolite Y, *J. Phys. Chem. B* 103 (1999) 647.
- [102] R. Vijayalakshmi, S. K. Kulshreshtha, Study of  $[\text{Fe}^{\text{II}}(\text{bpy})_3]^{2+}$  Complex Encapsulated in Zeolite Y, *Microp. Mesop. Mater.* 111 (2008) 449.
- [103] G. Vankó, Z. Homonnay, S. Nagy, A. Vértés, G. Pál-Borbély, H. K. Beyer, On the synthesis and steric distortion of the tris(2,2-bipyridine)iron(II)complex ion in zeolite-Y, *Chem. Commun.* (1996) 785.
- [104] K. Morokuma, Why Do Molecules Interact? The Origin of Electron Donor-Acceptor Complexes, Hydrogen Bonding and Proton Affinity, *Acc. Chem. Res.* 10 (1977) 294–300.
- [105] G. Vankó, S. Nagy, Z. Homonnay, A. Vértés, Sterical effects of encapsulation on some cobalt complexes built up in zeolite Y - A Mössbauer emission spectroscopy study, *Hyperfine Interact.* 126 (2000) 163.
- [106] A. Tissot, X. Kesse, S. Giannopoulou, I. Stenger, L. Binet, E. Rivière, C. Serre, A spin crossover porous hybrid architecture for potential sensing applications, *Chem. Commun.* 55 (2019) 194–197.
- [107] L. M. Lawson Daku, A. Hauser, *Ab Initio* Molecular Dynamics Study of an Aqueous Solution of  $[\text{Fe}(\text{bpy})_3](\text{Cl})_2$  in the Low-Spin and in the High-Spin State, *J. Phys. Chem. Lett.* 1 (2010) 1830.
- [108] L. M. Lawson Daku, Spin-state dependence of the structural and vibrational properties of solvated iron(II) polypyridyl complexes from aimd simulations: aqueous  $[\text{Fe}(\text{bpy})_3]\text{Cl}_2$ , a case study, *Phys.*

- Chem. Chem. Phys. 20 (2018) 6236–6253.
- [109] L. M. Lawson Daku, Spin-state dependence of the structural and vibrational properties of solvated iron(II) polypyridyl complexes from aimd simulations: II. aqueous  $[\text{Fe}(\text{tpy})_2]\text{Cl}_2$ , Phys. Chem. Chem. Phys. 21 (2019) 650–661.
- [110] M. Khalil, M. A. Marcus, A. L. Smeigh, J. K. McCusker, H. H. W. Chong, R. W. Schoenlein, Picosecond X-ray Absorption Spectroscopy of a Photoinduced Iron(II) Spin Crossover Reaction in Solution, J. Phys. Chem. A 110 (2006) 38–44.
- [111] W. Gawelda, V.-T. Pham, M. Benfatto, Y. Zaushitsyn, M. Kaiser, D. Grolimund, S. L. Johnson, R. Abela, A. Hauser, C. Bressler, M. Chergui, Structural Determination of a Short-Lived Excited Iron(II) Complex by Picosecond X-Ray Absorption Spectroscopy, Phys. Rev. Lett. 98 (2007) 057401.
- [112] W. Gawelda, V.-T. Pham, R. M. van der Veen, D. Grolimund, R. Abela, M. Chergui, C. Bressler, Structural analysis of ultrafast extended X-ray absorption fine structure with subpicometer spatial resolution: Application to spin crossover complexes, J. Chem. Phys. 130 (2009) 124520.
- [113] C. Bressler, C. Milne, V.-T. Pham, A. ElNahhas, R. M. van der Veen, W. Gawelda, S. Johnson, P. Beaud, D. Grolimund, M. Kaiser, C. N. Borca, G. Ingold, R. Abela, M. Chergui, Femtosecond XANES Study of the Light-Induced Spin Crossover Dynamics in an Iron(II) Complex, Science 323 (2009) 489–492.
- [114] G. Vankó, P. Glatzel, V.-T. Pham, R. Abela, D. Grolimund, C. N. Borca, S. L. Johnson, C. J. Milne, C. Bressler, Picosecond time-resolved x-ray emission spectroscopy: Ultrafast spin-state determination in an iron complex, Angew. Chem. Int. Ed. 49 (2010) 5910–5912.
- [115] S. Nozawa, T. Sato, M. Chollet, K. Ichiyanagi, A. Tomita, H. Fujii, S. ichi Adachi, S. ya Koshihara, Direct Probing of Spin State Dynamics Coupled with Electronic and Structural Modifications by Picosecond Time-Resolved XAFS, J. Am. Chem. Soc. 132 (2010) 61–63.
- [116] N. Huse, T. K. Kim, L. Jamula, J. K. McCusker, F. M. F. de Groot, R. W. Schoenlein, Photo-induced spin-state conversion in solvated transition metal complexes probed via time-resolved soft X-ray spectroscopy, J. Am. Chem. Soc. 132 (2010) 6809–6816.
- [117] N. Huse, H. Cho, K. Hong, L. Jamula, F. M. F. de Groot, T. K. Kim, J. K. McCusker, R. W. Schoenlein, Femtosecond soft X-ray spectroscopy of solvated transition-metal complexes: Deciphering the interplay of electronic and structural dynamics, J. Phys. Chem. Lett. 2 (2011) 880–884.
- [118] K. Haldrup, G. Vankó, W. Gawelda, A. Galler, G. Doumy, A. M. March, E. P. Kanter, A. Bordage, A. Dohn, T. B. van Driel, K. S. Kjær, H. T. Lemke, S. E. Canton, J. Uhlig, V. Sundström, L. Young, S. H. Southworth, M. M. Nielsen, C. Bressler, Guest–host interactions investigated by time-resolved X-ray spectroscopies and scattering at MHz rates: Solvation dynamics and photoinduced spin transition in aqueous  $\text{Fe}(\text{bipy})_3^{2+}$ , J. Phys. Chem. A 116 (2012) 9878–9887.
- [119] H. T. Lemke, C. Bressler, L. X. Chen, D. M. Fritz, K. J. Gaffney, A. Galler, W. Gawelda, K. Haldrup, R. W. Hartsock, H. Ihee, J. Kim, K. H. Kim, J. H. Lee, M. M. Nielsen, A. B. Stickrath, W. Zhang, D. Zhu, M. Cammarata, Femtosecond X-ray absorption spectroscopy at a hard X-ray free electron laser: Application to spin crossover dynamics, J. Phys. Chem. A 117 (2013) 735–740.
- [120] S. E. Canton, X. Zhang, L. M. Lawson Daku, A. L. Smeigh, J. Zhang, Y. Liu, C.-J. Wallentin, K. Attenkofer, G. Jennings, C. A. Kurtz, D. Gosztola, K. Wärnmark, A. Hauser, V. Sundström, Probing the anisotropic distortion of photoexcited spin crossover complexes with picosecond x-ray

- absorption spectroscopy, *J. Phys. Chem. C* 118 (2014) 4536–4545. doi:10.1021/jp5003963.
- [121] W. Zhang, R. Alonso-Mori, U. Bergmann, C. Bressler, M. Chollet, A. Galler, W. Gawelda, R. G. Hadt, R. W. Hartsock, T. Kroll, K. S. Kjaer, K. Kubicek, H. T. Lemke, H. W. Liang, D. A. Meyer, M. M. Nielsen, C. Purser, J. S. Robinson, E. I. Solomon, Z. Sun, D. Sokaras, T. B. van Driel, G. Vanko, T.-C. Weng, D. Zhu, K. J. Gaffney, Tracking excited-state charge and spin dynamics in iron coordination complexes, *Nature* 509 (7500) (2014) 345–348.
- [122] X. Zhang, M. L. Lawson Daku, J. Zhang, K. Suarez-Alcantara, G. Jennings, C. A. Kurtz, S. E. Canton, Dynamic jahn–teller effect in the metastable high-spin state of solvated  $[\text{Fe}(\text{terpy})_2]^{2+}$ , *J. Phys. Chem. C* 119 (2015) 3312–3321. doi:10.1021/jp5117068.
- [123] S. E. Canton, X. Zhang, M. L. Lawson Daku, Y. Liu, J. Zhang, S. Alvarez, Mapping the ultrafast changes of continuous shape measures in photoexcited spin crossover complexes without long-range order, *J. Phys. Chem. C* 119 (2015) 3322–3330. doi:10.1021/jp5117189.
- [124] G. Vankó, A. Bordage, M. Pápai, K. Haldrup, P. Glatzel, A. M. March, G. Doumy, A. Britz, A. Galler, T. Assefa, D. Cabaret, A. Juhin, T. B. van Driel, K. S. Kjær, A. Dohn, K. B. Møller, H. T. Lemke, E. Gallo, M. Rovezzi, Z. Németh, E. Rozsályi, T. Rozgonyi, J. Uhlig, V. Sundström, M. M. Nielsen, L. Young, S. H. Southworth, C. Bressler, W. Gawelda, Detailed characterization of a nanosecond-lived excited state: X-ray and theoretical investigation of the quintet state in photoexcited  $[\text{Fe}(\text{terpy})_2]^{2+}$ , *J. Phys. Chem. C* 119 (11) (2015) 5888–5902. doi:10.1021/acs.jpcc.5b00557.
- [125] K. Haldrup, W. Gawelda, R. Abela, R. Alonso-Mori, U. Bergmann, A. Bordage, M. Cammarata, S. E. Canton, A. O. Dohn, T. B. van Driel, D. M. Fritz, A. Galler, P. Glatzel, T. Harlang, K. S. Kjær, H. T. Lemke, K. B. Møller, Z. Németh, M. Pápai, N. Sas, J. Uhlig, D. Zhu, G. Vankó, V. Sundström, M. M. Nielsen, C. Bressler, Observing solvation dynamics with simultaneous femtosecond X-ray emission spectroscopy and X-ray scattering, *J. Phys. Chem. B* 120 (6) (2016) 1158–1168. doi:10.1021/acs.jpcc.5b12471.
- [126] B. E. Van Kuiken, H. Cho, K. Hong, M. Khalil, R. W. Schoenlein, T. K. Kim, N. Huse, Time-resolved x-ray spectroscopy in the water window: Elucidating transient valence charge distributions in an aqueous  $\text{Fe}(\text{II})$  complex, *J. Phys. Chem. Lett.* 7 (3) (2016) 465–470. doi:10.1021/acs.jpcclett.5b02509.
- [127] H. T. Lemke, K. S. Kjær, R. Hartsock, T. B. van Driel, M. Chollet, J. M. Glowacka, S. Song, D. Zhu, E. Pace, S. F. Matar, M. M. Nielsen, M. Benfatto, K. J. Gaffney, E. Collet, M. Cammarata, Coherent structural trapping through wave packet dispersion during photoinduced spin state switching, *Nat. Commun.* 8 (2017) 15342.
- [128] C. Liu, J. Zhang, L. M. Lawson Daku, D. Gosztola, S. E. Canton, X. Zhang, Probing the impact of solvation on photoexcited spin crossover complexes with high-precision X-ray transient absorption spectroscopy, *J. Am. Chem. Soc.* 139 (48) (2017) 17518–17524. doi:10.1021/jacs.7b09297.
- [129] J. E. Monat, J. K. McCusker, Femtosecond Excited-State Dynamics of an Iron(II) Polypyridyl Solar Cell Sensitizer Model, *J. Am. Chem. Soc.* 122 (2000) 4092–4097.
- [130] W. Gawelda, A. Cannizzo, V.-T. Pham, F. van Mourik, C. Bressler, M. Chergui, Ultrafast Nonadiabatic Dynamics of  $[\text{Fe}^{\text{II}}(\text{bpy})_3]^{2+}$  in Solution, *J. Am. Chem. Soc.* 129 (2007) 8199–8206.
- [131] A. L. Smeigh, M. Creelman, R. A. Mathies, J. K. McCusker, Femtosecond Time-Resolved Optical and Raman Spectroscopy of Photoinduced Spin Crossover: Temporal Resolution of Low-to-High Spin Optical Switching, *J. Am. Chem. Soc.* 130 (2008) 14105–14107.

- [132] A. Lapini, P. Foggi, L. Bussotti, R. Righini, A. Dei, Relaxation dynamics in three polypyridyl iron(II)-based complexes probed by nanosecond and sub-picosecond transient absorption spectroscopy, *Inorg. Chim. Acta* 361 (2008) 3937–3943.
- [133] C. Consani, M. Prémont-Schwarz, A. ElNahas, C. Bressler, F. van Mourik, A. Cannizzo, M. Chergui, Vibrational Coherences and Relaxation in the High-Spin State of Aqueous  $[\text{Fe}^{\text{II}}(\text{bpy})_3]^{2+}$ , *Angew. Chem. Int. Ed.* 48 (2009) 7184–7187.
- [134] G. Auböck, M. Chergui, Sub-50-fs photoinduced spin crossover in  $[\text{Fe}(\text{bpy})_3]^{2+}$ , *Nature Chem.* 7 (2015) 629–633.
- [135] A. Moguelevski, M. Wilke, G. Grell, S. I. Bokarev, S. G. Aziz, N. Engel, A. A. Raheem, O. KÄEhn, I. Y. Kiyani, E. F. Aziz, Ultrafast spin crossover in  $[\text{Fe}^{\text{II}}(\text{bpy})_3]^{2+}$ : Revealing two competing mechanisms by extreme ultraviolet photoemission spectroscopy, *ChemPhysChem* 18 (5) (2016) 465–469. doi:10.1002/cphc.201601396.
- [136] C. Brady, P. L. Callaghan, Z. Ciunik, C. G. Coates, A. Døssing, A. Hazell, J. J. McGarvey, S. Schenker, H. Toftlund, A. X. Trautwein, H. Winkler, J. A. Wolny, Molecular Structure and Vibrational Spectra of Spin-Crossover Complexes in Solution and Colloidal Media: Resonance Raman and Time-Resolved Resonance Raman Studies, *Inorg. Chem.* 43 (2004) 4289–4299.
- [137] M. M. N. Wolf, C. S. R. Groß, J. A. Wolny, V. Schünemann, A. Døssing, H. Paulsen, J. J. McGarvey, R. Diller, Sub-picosecond time resolved infrared spectroscopy of high-spin state formation in Fe(II) spin crossover complexes, *Phys. Chem. Chem. Phys.* 10 (2008) 4264–4273.
- [138] S. Iuchi, A model electronic hamiltonian to study low-lying electronic states of  $[\text{Fe}(\text{bpy})_3]^{2+}$  in aqueous solution, *J. Chem. Phys.* 136 (6) (2012) 064519. doi:10.1063/1.3684239.
- [139] A. K. Das, R. V. Solomon, F. Hofmann, M. Meuwly, Inner-shell water rearrangement following photoexcitation of Tris(2,2'-bipyridine)iron(II), *J. Phys. Chem. B* 120 (1) (2016) 206–216. doi:10.1021/acs.jpcc.5b10980.
- [140] S. Iuchi, N. Koga, Insight into the light-induced spin crossover of  $[\text{Fe}(\text{bpy})_3]^{2+}$  in aqueous solution from molecular dynamics simulation of d-d excited states, *Phys. Chem. Chem. Phys.* 18 (2016) 4789–4799. doi:10.1039/C5CP06406F.
- [141] M. Abedi, G. Levi, D. B. Zederkof, N. E. Henriksen, M. Pápai, K. B. Møller, Excited-state solvation structure of transition metal complexes from molecular dynamics simulations and assessment of partial atomic charge methods, *Phys. Chem. Chem. Phys.* 21 (2019) 4082–4095. doi:10.1039/C8CP06567E.
- [142] D. Khakhulin, L. M. Lawson Daku, D. Leshchev, G. E. Newby, M. Jarenmark, C. Bressler, M. Wulff, S. E. Canton, Visualizing the coordination-spheres of photoexcited transition metal complexes with ultrafast hard X-rays, *Phys. Chem. Chem. Phys.* 21 (2019) 9277–9284. doi:10.1039/C9CP01263J.